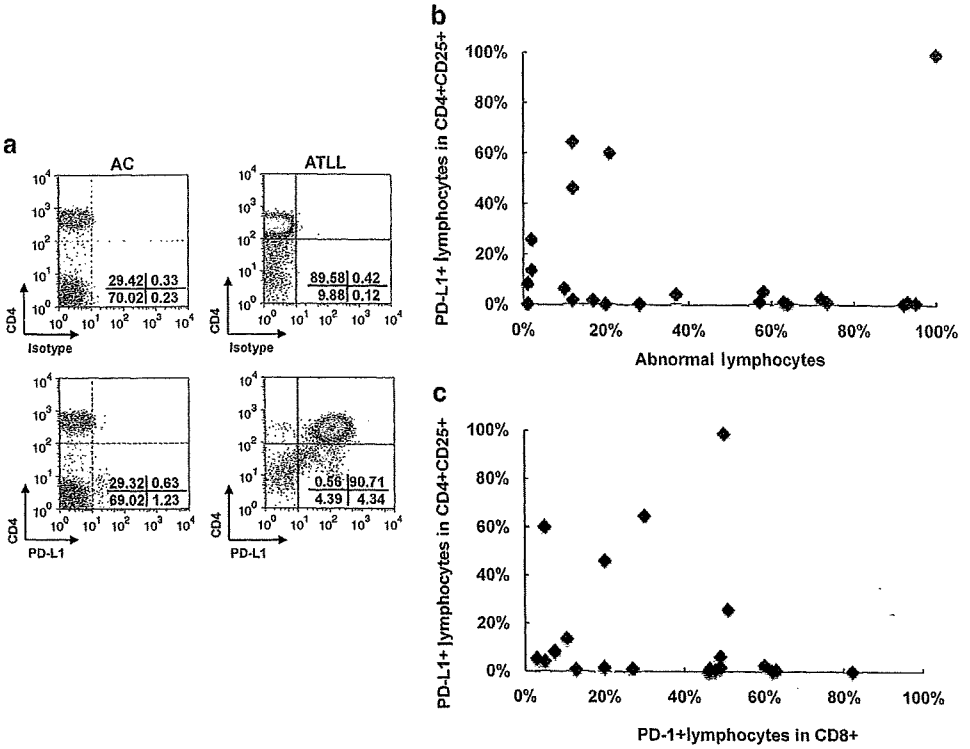

Figure 2 Programmed death-ligand 1 (PD-L1) expression on lymphocytes in asymptomatic HTLV-1 carriers (ACs) and adult T-cell leukemia/lymphoma (ATLL) patients. (**a**) Representative flow cytometric plots of PD-L1 expression in AC and ATLL patients. Numbers indicate the percentages in lymphocytes. (**b**) Percentages of PD-L1 expression on CD4+25+ lymphocytes in AC and ATLL along with the percentage of abnormal lymphocytes in peripheral blood. (**c**) Percentages of PD-L1 expression on CD4+25+ lymphocytes in AC and ATLL along with the percentage of programmed death-1 (PD-1)+ lymphocytes in CD8+ cells.

ligand of this axis, PD-L1 expression was measured. Freshly isolated or cryopreserved PBMCs from 16 ACs, 23 ATLL patients and 17 HDs were stained for PD-L1 expression in combination with CD4 and CD25 expression. Representative PD-L1+ staining patterns on CD4+-gated lymphocytes are shown in Figure 2a. The percentage of PD-L1 expression on CD4+CD25 cells was summarized in Figure 2b along with the percentage of abnormal lymphocytes in peripheral blood. There was no correlation between the percentage of PD-L1 expression on CD4+CD25 cells and the percentage of abnormal lymphocytes in peripheral blood. Lymphocytes from ACs were negative for PD-L1 expression (mean = 0.3 ± 0.57%, data not shown), whereas 5 of 23 ATLL patients (21.7%) showed higher rates of PD-L1 expression on lymphocytes (mean = 11.6 ± 27.8%, Figure 2b). Among HDs, the percentage of lymphocytes expressing PD-L1 was 0.43 ± 0.62 (data not shown). PD-L1 expression on the CD4+CD25 lymphocytes appeared to vary among individuals. Such variation is also seen *in vitro*; the cloned HTLV-1-infected Oh13T cell line and HTLV-1-negative Jurkat cell line expressed PD-L1, whereas HTLV-1-infected Su9TO1, K3T, F6T, SIT[38] and HTLV-1-negative MOLT-4 and KG-1 had no measurable PD-L1 expression (data not shown). The percentage of PD-L1 expression on CD4+CD25+ cells was summarized in Figure 2c along with the percentage of PD-1 expression in CD8+ lymphocytes. There was no correlation between the percentage of PD-L1 expression on CD4+CD25 cells and the percentage of PD-1 expression in CD8+ lymphocytes. We compared the clinical characteristics of two groups of ATLL cases, in which one group showed high expression and the other showed low expression of PD-L1 on ATLL cells. There are no differences between those groups in terms of chemosensitivity, survival, hypercalcemia, LDH, percentage of ATLL cells in peripheral blood and involvement of other organs. However, PD-L1 expression was not observed in the CD4+CD25+ cells at diagnosis in all ATLL patients. Samples from all the five patients who express high PD-L1 on CD4+CD25+ cells (>10%) were collected at least 12 months after diagnosis (21.0 ± 15.3 months). Three of the five patients were severely refractory to chemotherapy, and the other two patients were in chronic stage.

To explore whether PD-L1 expression occurs on HTLV-1-infected cells, we examined T cells expressing Tax, an HTLV-1 oncoprotein. PD-L1 expression was observed on PBMCs cultured for 12 h from ACs (6 of 7), but not from HDs (0 of 6, representative data shown in Figure 3). Overall, 84.7% of the HTLV-1 Tax+ cultured cells expressed PD-L1, although there was no HTLV-1 Tax expression on cells freshly isolated from ACs. Interestingly, all HTLV-1 Tax+PD-L1+lymphocytes were CD4+CD25+ (data not shown). Thus, HTLV-1-infected cells were conditionally capable of inducing PD-L1 expression.

Blockade of the PD-1/PD-L1 pathway enhances CD8+ T-cell function

To assess whether PD-1 expression on CD8+ lymphocytes from ACs and ATLL patients could affect function, cytolytic reactions were performed using flow cytometric quantification of intracellular IFN-γ and TNF-α produced in HTLV-1 Tax-specific CD8+ cells. These cytokines are primarily produced by activated lymphocytes and act as multifunctional immunomodulators with antitumor and antiviral activity.[31] Representative results regarding IFN-γ, TNF-α and CD107a production are

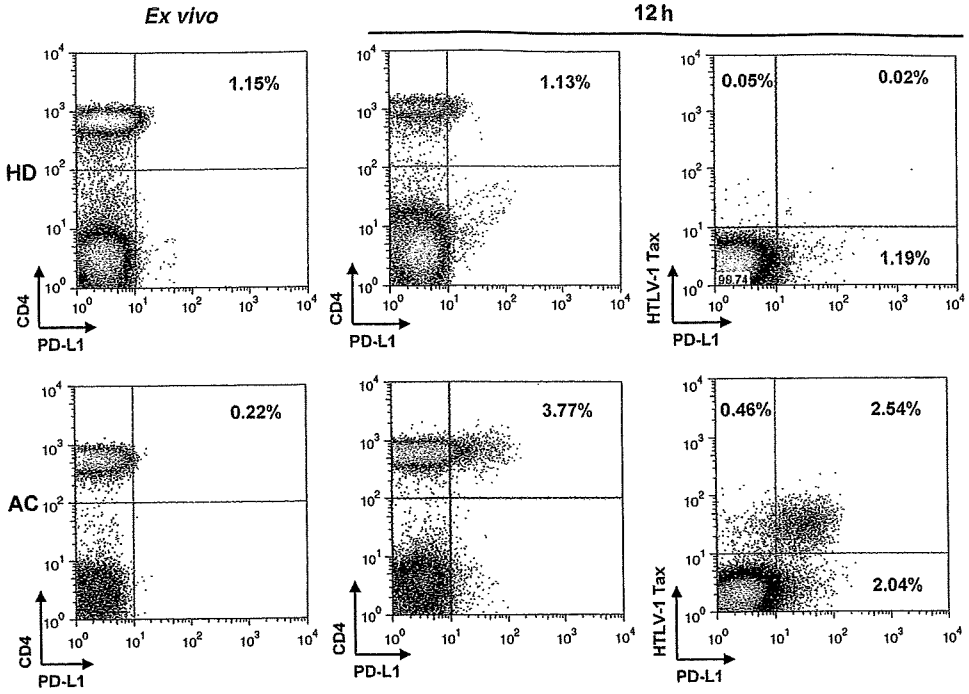

Figure 3 Human T-cell leukemia virus-1 (HTLV-1)-infected cells are capable of inducing programmed death-ligand 1 (PD-L1). Representative flow cytometric plots of PD-L1 expression gated by lymphocytes in healthy donor (HD) (upper) and asymptomatic HTLV-1 carrier (AC) (lower). The left panel shows the results obtained *ex vivo*, whereas the right panel shows those after 12 h in culture gated by lymphocytes. Increases in PD-L1 expression were observed after cultivation in AC but not in HD. The numbers indicate the percentage of lymphocytes. The figure shows one representative result of PD-L1 expression in six HDs and seven ACs. There was no HTLV-1 Tax expression *ex vivo*. All HTLV-1 Tax+PD-L1+lymphocytes were CD4+CD25+cells.

shown in Figure 4a. We incubated freshly isolated PBMCs from ACs and ATLL patients in culture medium alone or medium containing anti-PD-L1 antibody in the presence or absence of HTLV-1 Tax peptide for 6 or 16 h. Intracellular cytokine+ cells were estimated from HTLV-1-tetramer+CD8+ T lymphocytes. The HTLV-1 Tax peptide tetramer+ CD8+ T cells produced only low levels of IFN-γ, TNF-α and CD107a after short-term cultures in the absence of HTLV-1 Tax peptide (<0.6, <1.0 and <0.8%, respectively). However, the percentage of cells producing IFN-γ when incubated in the presence of Tax peptide increased to 24.1±20.2% in the tetramer+CD8+ T cells (Figure 4a), whereas the percentage of cells producing IFN-γ when incubated in the presence of anti-PD-L1 antibody increased to 29.0±21.7% ($P<0.05$). The percentage of cells expressing TNF-α when incubated with HTLV-1 Tax peptide increased to 14.0±7.4% in the tetramer+CD8+ T cells, whereas the percentage of cells producing TNF-α in the presence of anti-PD-L1 antibody increased to 20.0±11.9% ($P<0.05$). CD107a expression with added HTLV-1 Tax peptide increased to 36.8±18.5% of the tetramer+CD8+ T cells, whereas CD107a expression in the presence of the anti-PD-L1 antibody increased to 42.2±15.8% ($P<0.05$). Thus, stimulation with HTLV-1 Tax peptide in the presence of PD-L1 antibody further enhanced IFN-γ, TNF-α production and CD107a expression, which were significantly increased in those in tetramer-positive cells, when compared with peptide-only stimulation in ACs and ATLL patients ($P<0.05$, Figure 4b). There was no different PD-L1 blockage response between the tetramer+ CD8+ functional molecule+ from the ACs and ATLL patients. Interfering with the PD-1/PD-L1 pathway using an anti-PD-L1 antibody enhanced the production of IFN-γ, TNF-α and expression of CD107a on HTLV-1 tetramer-positive CD8+ cells, indicating the restored function of HTLV-1-specific CD8+ cells.

Discussion

A higher percentage of PD-1 expression was observed on total and CD8+ T cells in ACs compared with HDs (Figure 1b). Although no earlier study of other oncogenic viruses has shown a correlation between PD-1 expression and the carrier state or eventual progression to cancer, in this study, we report that the percentage of CD8+ lymphocytes expressing PD-1 was higher for ATLL patients compared with ACs (Figure 1b). Even though we failed to measure HTLV-I provirus load with those samples, this may reflect the higher load of virus-associated antigens in ATLL patients than in ACs, as it has also been shown that the PD-1 expression is increased in HIV viremic compared with aviremic individuals.[27] Indeed, our Tax data here (Figure 3) indicate that there may be some correlation between these effects. The observation of fairly high rates of PD-1 expression on CD8+ lymphocytes in ATLL patients and ACs compared with HDs prompted us to investigate PD-1 expression on viral antigen-specific CTL from ATLL patients, ACs and HDs. PD-1 expression on HTLV-1-specific CD8+ lymphocytes from ACs was just as high as that observed on cells from ATLL patients, whereas PD-1 expression on CMV- and EBV-tetramer-positive CD8+ lymphocytes was also upregulated, but to a lesser extent than on cells from in ATLL patients (Figure 1c). These observations suggest relatively skewed exhaustion of CTLs against HTLV-1 more than against other viruses in the carrier state, which is consistent with the observation that ATLL patients show a broadly compromised immune system.[11,39] This may be

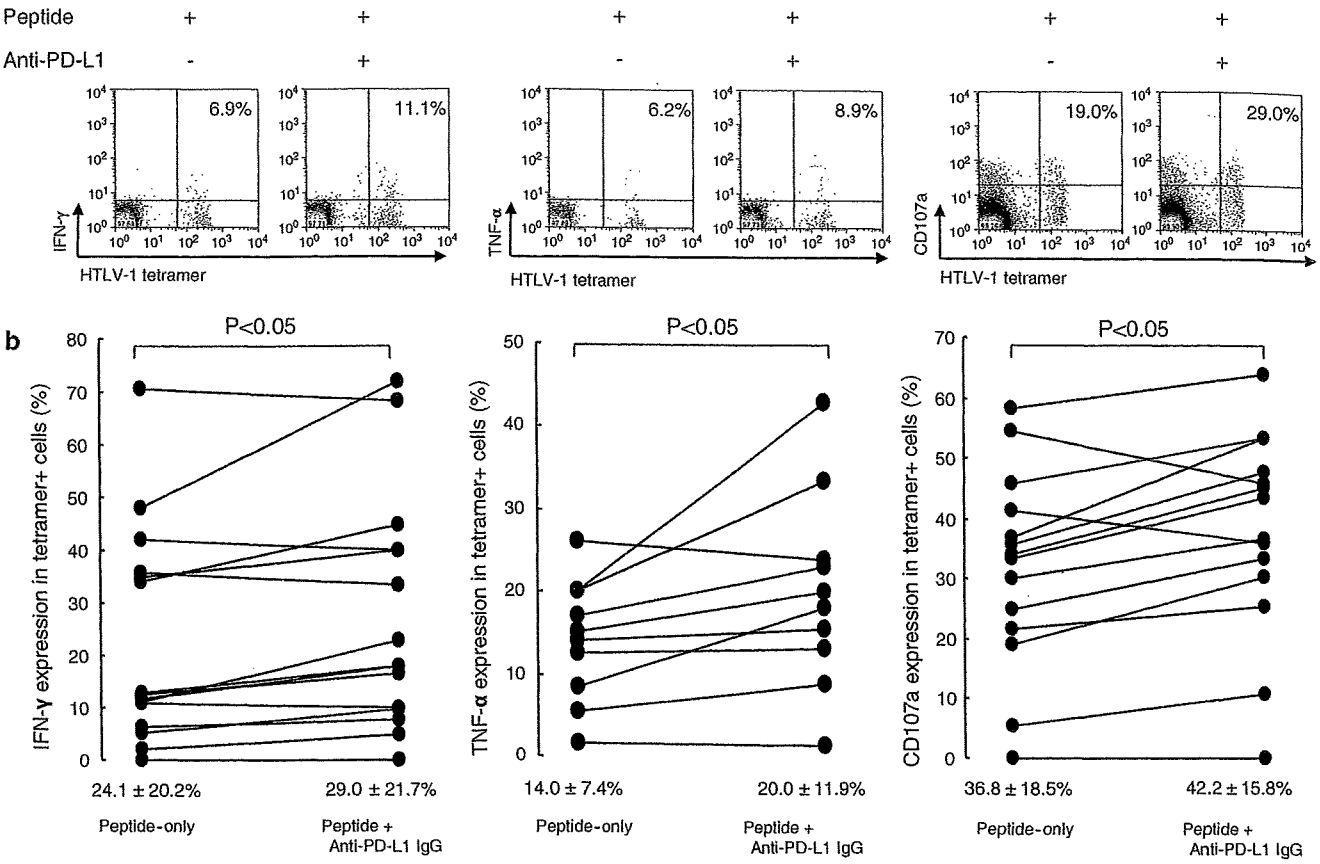

Figure 4 Blocking the programmed death-1/programmed death-ligand 1 (PD-1/PD-L1) pathway increases cytolytic reaction in human T-cell leukemia virus-1 (HTLV-1)-specific CD8+ cells. (**a**) Representative flow cytometric plots of interferon-γ (IFN-γ), tumor necrosis factor-α (TNF-α) and CD107a expression in HTLV-1-specific CD8+ T cells are shown. The numbers indicate the percentages in HTLV-1-specific CD8+ T lymphocytes. The left panel shows the results in the presence of 0.02 μM peptide, whereas the right panel shows peptide treatment in the presence of anti-PD-L1 blocking antibody. (**b**) Percentage of intracellular IFN-γ, TNF-α and CD107a expression in HTLV-1-specific CD8+ T lymphocytes treated with peptide and with anti-PD-L1 IgG. The numbers represent the means ± s.d. Statistical comparisons were made using the Wilcoxon-matched pair test.

one factor facilitating the persistence of HTLV-1-infected cells even in the presence of anti-HTLV-1 antigen-specific CTL. Furthermore, PD-1 expression on HTLV-1-specific CD8+ T cells was unique as we did not see upregulation of the inhibitory receptor CTL antigen-4 (data not shown) on CD8+ T cells, consistent with earlier reports related to HIV infection.[25,40]

The interaction of PD-1 with PD-L1 has been shown to negatively regulate the cytokine production and proliferation of T cells, allowing tumor evasion of the host immune system by negative attenuation of tumor-specific T-cell responses.[19,23] PD-L1 expression is found on many solid tumors, and increased expression of PD-L1 is associated with poor prognosis.[19,22,41] In this study, we showed that some primary ATLL cells express PD-L1 on the cell surface (Figure 2); however, the expression patterns varied considerably between individual patients. Notably, none of the ATLL patients expressed PD-L1 at diagnosis on ATLL cells in this cohort. Samples from all five patients who express high PD-L1 on CD4+CD25+ cells (>10%) were collected at least 12 months after diagnosis. Shimauchi *et al.*[42] also reported that CD4+CD25+ tumor cells expressed a low but discernible level of PD-L1 in only one of four cases. This and our data are in contrast with an earlier study that assessed PD-L1 expression in 30 heterogenous acute leukemia patients and found that 57% of patients expressed PD-L1 at diagnosis on leukemic cells.[43] The serial measurement of PD-L1 expression on ATLL cells clearly needs to be carried out to determine the significance of PD-L1 expression for the disease characteristics.

Nakanishi *et al.*[44] reported increased PD-1 expression on tumor-infiltrating lymphocytes; however, the specificity of tumor-infiltrating lymphocytes against tumor-associated antigens was not addressed because of technical limitations. In our study, we assessed CTL specific to HTLV-1, which is a tumor-causing virus, using a well-established and highly sensitive tetramer assay. This may provide direct evidence that the PD-1/PD-L1 interaction is one of the mechanisms allowing ATLL evasion from the host immune system. Although approximately 60% of ATLL cells do not express Tax protein *in vivo*,[7] it has been reported that HTLV-1 Tax-specific CD8+ lymphocytes play an important role in ATLL tumor immunity after hematopoietic stem cell transplantation.[12] This tumor-associated antigen-specific tetramer assay will be used further to assess whether therapeutic intervention against the PD-1/PD-L1 pathway can restore PD-1-expressing CD8+ lymphocytes in a malignancy setting, as has been reported in chronic viral infection models.[25] Although some ATLL cells from uncultured peripheral blood did not express PD-L1, we found that HTLV-1-infected cells are capable of producing PD-L1 in short-term

culture assays (Figure 3). PD-1 expression in HTLV-1-specific CD8+ T cells in ACs and ATLL patients is similarly increased. These results suggest that interaction of high PD-1 expression on HTLV-1-specific CD8+ T cells could occur with PD-L1 in ATLL patients. Indeed, an earlier study has shown that PD-L1 is upregulated in HIV-infected individuals;[26] yet, to date, it is unknown whether HIV-infected cells that express viral-derived protein are capable of producing PD-L1.

Our earlier study revealed that HTLV-1-specific CD8+ T cells, which produce intracellular molecules relevant to cytolytic effector function (IFN-γ, perforin and granzyme B), are lacking in effector functions in ATLL patients.[13] Here, we also examined whether interrupting the ligation of PD-1 by its ligand PD-L1 could increase the cytolytic potential of HTLV-1-specific CD8+ T cells, similar to reports in a mouse model *in vivo* using cells from glioma and HIV patients *in vitro*.[24,25,27,41] Our results showed that blockade of the PD-1/PD-L1 pathway augmented the production of IFN-γ, TNF-α and expression of the degranulation marker, CD107a, by effector cells. Blank *et al*.[21] also reported that blockade of endogenous PD-L1 expression on human cancer cells can still improve the immune functions of tumor-specific T cells *in vitro*. Furthermore, Maier *et al*.[45] reported that blockade of PD-1/PD-L1 pathways may reverse viral persistence and chronic infection in cases, in which the CTL secretion of IFN-γ, after antigen recognition in the liver is suppressed. Taken together, the results of these studies suggest that an effective blockade of PD-L1 interactions with immune effector cells *in vivo* may provide a promising strategy of immunotherapy for selected tumors expressing PD-L1.[14,21,23]

In summary, this study indicates that the immunoregulatory PD-1/PD-L1 pathway is operative during persistent viral infection, and suggests that this pathway may contribute to exhaustion of the CTL response in HTLV-1-infected individuals, which may facilitate immune evasion and ATLL development. Furthermore, interventions that lead to reactivation of exhausted T cells by blocking the PD-1/PD-L1 axis may be an effective immunological strategy for the clearance of persistent HTLV-1 infection and the treatment of ATLL.

Acknowledgements

Research support: This study was supported by a Grant-in-Aid (to NA) from the Japanese Ministry of Health, Labor, and Welfare, and by the Kagoshima University for Frontier Science Research Center Program (to NA). We thank Dr Jeffrey A Medin for a critical reading of the paper, Ms Hokkoku for preparation of clinical samples, and Ms Ariyoshi for HLA typing.

References

1 Uchiyama T. Human T cell leukemia virus type I (HTLV-I) and human diseases. *Annu Rev Immunol* 1997; **15**: 15–37.
2 Popovic M, Reitz Jr MS, Sarngadharan MG, Robert-Guroff M, Kalyanaraman VS, Nakao Y *et al*. The virus of Japanese adult T-cell leukaemia is a member of the human T-cell leukaemia virus group. *Nature* 1982; **300**: 63–66.
3 Yoshida M. Multiple viral strategies of HTLV-1 for dysregulation of cell growth control. *Annu Rev Immunol* 2001; **19**: 475–496.
4 Verdonck K, Gonzalez E, Van Dooren S, Vandamme AM, Vanham G, Gotuzzo E. Human T-lymphotropic virus 1: recent knowledge about an ancient infection. *Lancet Infect Dis* 2007; **7**: 266–281.
5 Taylor GP, Matsuoka M. Natural history of adult T-cell leukemia/lymphoma and approaches to therapy. *Oncogene* 2005; **24**: 6047–6057.
6 Tsukasaki K, Utsunomiya A, Fukuda H, Shibata T, Fukushima T, Takatsuka Y *et al*. VCAP-AMP-VECP compared with biweekly CHOP for adult T-cell leukemia-lymphoma: Japan Clinical Oncology Group Study JCOG9801. *J Clin Oncol* 2007; **25**: 5458–5464.
7 Yamada Y, Tomonaga M, Fukuda H, Hanada S, Utsunomiya A, Tara M *et al*. A new G-CSF-supported combination chemotherapy, LSG15, for adult T-cell leukaemia-lymphoma: Japan Clinical Oncology Group Study 9303. *Br J Haematol* 2001; **113**: 375–382.
8 Yasunaga J, Matsuoka M. Human T-cell leukemia virus type I induces adult T-cell leukemia: from clinical aspects to molecular mechanisms. *Cancer Control* 2007; **14**: 133–140.
9 Proietti FA, Carneiro-Proietti AB, Catalan-Soares BC, Murphy EL. Global epidemiology of HTLV-I infection and associated diseases. *Oncogene* 2005; **24**: 6058–6068.
10 Matsuoka M, Jeang KT. Human T-cell leukaemia virus type 1 (HTLV-1) infectivity and cellular transformation. *Nat Rev Cancer* 2007; **7**: 270–280.
11 Arnulf B, Thorel M, Poirot Y, Tamouza R, Boulanger E, Jaccard A *et al*. Loss of the *ex vivo* but not the reinducible CD8+ T-cell response to Tax in human T-cell leukemia virus type 1-infected patients with adult T-cell leukemia/lymphoma. *Leukemia* 2004; **18**: 126–132.
12 Kannagi M, Harashima N, Kurihara K, Ohashi T, Utsunomiya A, Tanosaki R *et al*. Tumor immunity against adult T-cell leukemia. *Cancer Sci* 2005; **96**: 249–255.
13 Kozako T, Arima N, Toji S, Masamoto I, Akimoto M, Hamada H *et al*. Reduced frequency, diversity, and function of human T cell leukemia virus type 1-specific CD8+ T cell in adult T cell leukemia patients. *J Immunol* 2006; **177**: 5718–5726.
14 Blank C, Mackensen A. Contribution of the PD-L1/PD-1 pathway to T-cell exhaustion: an update on implications for chronic infections and tumor evasion. *Cancer Immunol Immunother* 2007; **56**: 739–745.
15 Greenwald RJ, Freeman GJ, Sharpe AH. The B7 family revisited. *Annu Rev Immunol* 2005; **23**: 515–548.
16 Sharpe AH, Wherry EJ, Ahmed R, Freeman GJ. The function of programmed cell death 1 and its ligands in regulating autoimmunity and infection. *Nat Immunol* 2007; **8**: 239–245.
17 Okazaki T, Honjo T. Rejuvenating exhausted T cells during chronic viral infection. *Cell* 2006; **124**: 459–461.
18 Nishimura H, Minato N, Nakano T, Honjo T. Immunological studies on PD-1 deficient mice: implication of PD-1 as a negative regulator for B cell responses. *Int Immunol* 1998; **10**: 1563–1572.
19 Brown JA, Dorfman DM, Ma FR, Sullivan EL, Munoz O, Wood CR *et al*. Blockade of programmed death-1 ligands on dendritic cells enhances T cell activation and cytokine production. *J Immunol* 2003; **170**: 1257–1266.
20 Freeman GJ, Long AJ, Iwai Y, Bourque K, Chernova T, Nishimura H *et al*. Engagement of the PD-1 immunoinhibitory receptor by a novel B7 family member leads to negative regulation of lymphocyte activation. *J Exp Med* 2000; **192**: 1027–1034.
21 Blank C, Kuball J, Voelkl S, Wiendl H, Becker B, Walter B *et al*. Blockade of PD-L1 (B7-H1) augments human tumor-specific T cell responses *in vitro*. *Int J Cancer* 2006; **119**: 317–327.
22 Dong H, Chen L. B7-H1 pathway and its role in the evasion of tumor immunity. *J Mol Med* 2003; **81**: 281–287.
23 Iwai Y, Ishida M, Tanaka Y, Okazaki T, Honjo T, Minato N. Involvement of PD-L1 on tumor cells in the escape from host immune system and tumor immunotherapy by PD-L1 blockade. *Proc Natl Acad Sci USA* 2002; **99**: 12293–12297.
24 Barber DL, Wherry EJ, Masopust D, Zhu B, Allison JP, Sharpe AH *et al*. Restoring function in exhausted CD8T cells during chronic viral infection. *Nature* 2006; **439**: 682–687.
25 Day CL, Kaufmann DE, Kiepiela P, Brown JA, Moodley ES, Reddy S *et al*. PD-1 expression on HIV-specific T cells is associated with T-cell exhaustion and disease progression. *Nature* 2006; **443**: 350–354.
26 Trabattoni D, Saresella M, Biasin M, Boasso A, Piacentini L, Ferrante P *et al*. B7-H1 is up-regulated in HIV infection and is a novel surrogate marker of disease progression. *Blood* 2003; **101**: 2514–2520.
27 Trautmann L, Janbazian L, Chomont N, Said EA, Gimmig S, Bessette B *et al*. Upregulation of PD-1 expression on HIV-specific CD8+ T cells leads to reversible immune dysfunction. *Nat Med* 2006; **12**: 1198–1202.

28 Osame M, Nakagawa M, Umehara F, Ijichi S, Moritoyo T, Higuchi I *et al.* Recent studies on the epidemiology, clinical features and pathogenic mechanisms of HTLV-I associated myelopathy (HAM/TSP) and other diseases associated to HTLV. *J Neurovirol* 1997; **3** (Suppl 1): S50–S51.
29 Shimoyama M. Diagnostic criteria and classification of clinical subtypes of adult T-cell leukaemia-lymphoma. A report from the Lymphoma Study Group (1984–1987). *Br J Haematol* 1991; **79**: 428–437.
30 Kuzushima K, Hayashi N, Kimura H, Tsurumi T. Efficient identification of HLA-A*2402-restricted cytomegalovirus-specific CD8+ T-cell epitopes by a computer algorithm and an enzyme-linked immunospot assay. *Blood* 2001; **98**: 1872–1881.
31 Betts MR, Price DA, Brenchley JM, Lore K, Guenaga FJ, Smed-Sorensen A *et al.* The functional profile of primary human antiviral CD8+ T cell effector activity is dictated by cognate peptide concentration. *J Immunol* 2004; **172**: 6407–6417.
32 Altman JD, Moss PAH, Goulder PJR, Barouch DH, McHeyzer-Williams MG, Bell JI *et al.* Phenotypic analysis of antigen-specific T lymphocytes. *Science* 1996; **274**: 94–96.
33 Bodinier M, Peyrat MA, Tournay C, Davodeau F, Romagne F, Bonneville M *et al.* Efficient detection and immunomagnetic sorting of specific T cells using multimers of MHC class I and peptide with reduced CD8 binding. *Nat Med* 2000; **6**: 707–710.
34 Prussin C, Metcalfe DD. Detection of intracytoplasmic cytokine using flow cytometry and directly conjugated anti-cytokine antibodies. *J Immunol Methods* 1995; **188**: 117–128.
35 Kanai T, Totsuka T, Uraushihara K, Makita S, Nakamura T, Koganei K *et al.* Blockade of B7-H1 suppresses the development of chronic intestinal inflammation. *J Immunol* 2003; **171**: 4156–4163.
36 Saudemont A, Jouy N, Hetuin D, Quesnel B. NK cells that are activated by CXCL10 can kill dormant tumor cells that resist CTL-mediated lysis and can express B7-H1 that stimulates T cells. *Blood* 2005; **105**: 2428–2435.
37 Rubio V, Stuge TB, Singh N, Betts MR, Weber JS, Roederer M *et al.* *Ex vivo* identification, isolation and analysis of tumor-cytolytic T cells. *Nat Med* 2003; **9**: 1377–1382.
38 Arima N, Arimura K, Tokito Y, Sakaki Y, Matsushita K, Orihara K *et al.* HTLV-I Tax protein inhibits apoptosis induction but not G1 arrest by pyrrolidinedithiocarbamate, an anti-oxidant, in adult T cell leukemia cells. *Exp Hematol* 2004; **32**: 195–201.
39 Hirata T, Uchima N, Kishimoto K, Zaha O, Kinjo N, Hokama A *et al.* Impairment of host immune response against strongyloides stercoralis by human T cell lymphotropic virus type 1 infection. *Am J Trop Med Hyg* 2006; **74**: 246–249.
40 Steiner K, Waase I, Rau T, Dietrich M, Fleischer B, Broker BM. Enhanced expression of CTLA-4 (CD152) on CD4+ T cells in HIV infection. *Clin Exp Immunol* 1999; **115**: 451–457.
41 Wintterle S, Schreiner B, Mitsdoerffer M, Schneider D, Chen L, Meyermann R *et al.* Expression of the B7-related molecule B7-H1 by glioma cells: a potential mechanism of immune paralysis. *Cancer Res* 2003; **63**: 7462–7467.
42 Shimauchi T, Kabashima K, Nakashima D, Sugita K, Yamada Y, Hino R *et al.* Augmented expression of programmed death-1 in both neoplastic and non-neoplastic CD4+ T-cells in adult T-cell leukemia/lymphoma. *Int J Cancer* 2007; **121**: 2585–2590.
43 Salih HR, Wintterle S, Krusch M, Kroner A, Huang YH, Chen L *et al.* The role of leukemia-derived B7-H1 (PD-L1) in tumor-T-cell interactions in humans. *Exp Hematol* 2006; **34**: 888–894.
44 Nakanishi J, Wada Y, Matsumoto K, Azuma M, Kikuchi K, Ueda S. Overexpression of B7-H1 (PD-L1) significantly associates with tumor grade and postoperative prognosis in human urothelial cancers. *Cancer Immunol Immunother* 2007; **56**: 1173–1182.
45 Maier H, Isogawa M, Freeman GJ, Chisari FV. PD-1:PD-L1 interactions contribute to the functional suppression of virus-specific CD8+ T lymphocytes in the liver. *J Immunol* 2007; **178**: 2714–2720.

A second NOTCH1 chromosome rearrangement: t(9;14)(q34.3;q11.2) in T-cell neoplasia

Leukemia (2009) **23**, 1003–1006; doi:10.1038/leu.2008.366; published online 8 January 2009

NOTCH1 encodes a transmembrane signaling protein that plays key roles in development and neoplasia. Its leukemogenic involvement was first revealed by analysis of t(7;9)(q34;q34.3) in a T-cell acute lymphocytic leukemia (T-ALL) cell line (SUP-T1), which juxtaposes truncated NOTCH1 with TCRB, directing overexpression of N-terminally truncated polypeptides (reviewed in Grabher *et al*[1]). Wild-type NOTCH1 is initially cleaved (S1 cleavage) into twin polypeptides: an extracellular N-terminal subunit (NEC) and a transmembrane C-terminal

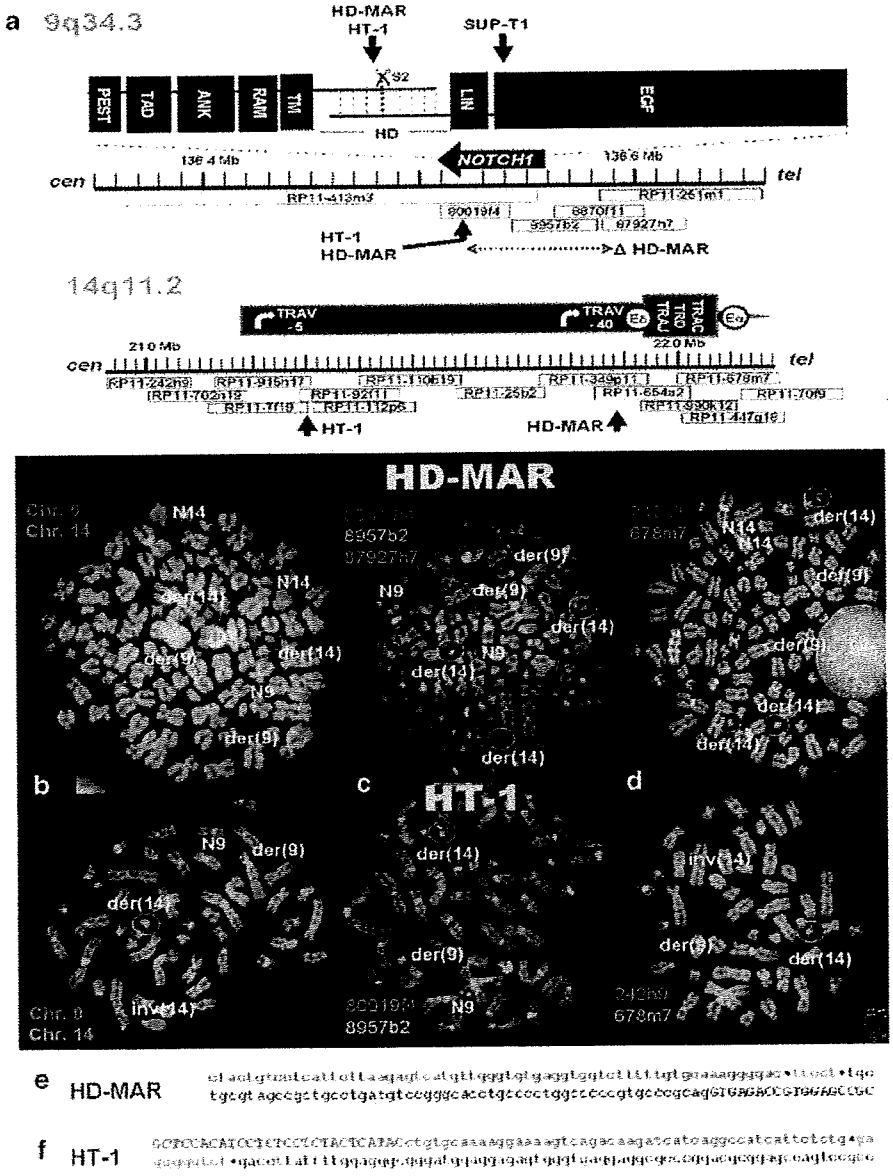

Figure 1 Cytogenetic and molecular breakpoint analysis of t(9;14)(q34;q11). (**a**) Breakpoint data, clone maps and the genomic structures of NOTCH1, including protein domain schema, and TRAD Note the intra-heterodimerization domain (HD) breakpoints in HD-MAR/HT-1 downstream of the S2 metalloprotease cleavage site, and the *cis*-HD breakpoint in SUP-T1. (**b**) Chromosome painting of t(9;14), and (**c** and **d**) FISH analyses of NOTCH1 and TRAD, respectively, in HD-MAR[4] and HT-1.[5] TRAD/NOTCH1 breakpoint junction sequences determined by long-distance inverse (LDI)-PCR are shown in (**e**) and (**f**), respectively. Nucleotides are shown in red, green and black to indicate TRAD, filler DNA and NOTCH1, respectively, with breakpoints shown as black dots. LDI-PCR was performed as described elsewhere.[6] Primer sequences are given in the Supplementary data.

subunit (NTM). Binding of NOTCH ligands to the epidermal growth factor-like repeats region of NEC promotes metalloprotease cleavage of NTM (S2 cleavage) to create membrane-bound NTM*I monomers (Figure 1a). These are cleaved in turn (S3 cleavage) at multiple sites within the heterodimerization domain (HD) binding extracellular and transmembrane subunits by the γ-secretase (GS) protease complex to release the intracellular domain (ICN1), which forms a ternary complex stimulating effector transcription.[1] ICN1 contains regulator of amino acid metabolism (RAM), ankyrin repeat and transcriptional activation domains, and a C-terminal polypeptide enriched with proline, glutamate, serine and threonine (PEST). Ankyrin and transcriptional activation domains are required for induction of T-ALL in mice.[2] Whereas γ-secretase inhibitors (GSi) may prove effective against T-ALL subsets, most T-cell lines are resistant, including SUP-T1.[3] We describe a second NOTCH1 rearrangement, t(9;14)(q34.3;q11.2), in T-ALL cell lines, HD-MAR[4] and HT-1,[5] both highly GSi-sensitive despite overexpressing truncated NOTCH1.

Cytogenetic analysis revealed t(9;14)(q34.3;q11.2) in both HD-MAR and HT-1 cells, with NOTCH1 breakpoints inside fosmid 80019F4 accompanied in HD-MAR cells by deletion of ~80 kbp corresponding to NEC (Figures 1a–d). Fluorescence *in situ* hybridization (FISH) also showed 14q11.2 breakpoints in both HD-MAR and HT-1 cells within the TRAV locus. These observations define an hitherto unlisted rearrangement (http://atlasgeneticsoncology.org//index.html), t(9;14)(q34.3;q11.2) that juxtaposes the intragenic regions of both NOTCH1 and TRAV. Long-distance inverse (LDI)-PCR confirmed and extended these findings, revealing tail-to-tail fusions of intron-27 of NOTCH1 at 138 516 818 and 138 516 905 bp, with 5′-TRAV40 (21 852 526 bp) and intron-1 of TRAV5 (21 287 494 bp) in HD-MAR and HT-1, respectively (Figures 1e and f, Supplementary Figure S1 A/B). t(9;14) in HD-MAR and HT-1 cells places NOTCH1, truncated inside HD (predicted 5 amino acids *trans-* of the S2 cleavage site), under transcriptional control of TRAV (Figure 1a). The TRAV-40 breakpoint in HD-MAR lies close to the proximal Eδ enhancer, whereas that in HT-1 at TRAV-5 lies ~600 kbp upstream near a cluster of DNase-I hypersensitive sites known to drive oncogene transcription in T-ALL. Thus, both t(9;14) cell lines carry breakpoints located inside HD, in contrast with that lying upstream (*cis-*) of HD in t(7;9) SUP-T1 cells.[1]

Protein (western blot) analyses of the minimal transforming regions, ankyrin and transcriptional activation domains, together with TM/RAM domains in T-ALL cells are shown in Figure 2a (top/middle). High protein expression of full-length NOTCH1 (~300 kDa) and NTM (~120 kDa) was detected in non-translocation cell lines excepting TALL-1 cells, which is monosomic for chromosome 9. Contrastingly, in NOTCH1 translocation cell lines the ~300-kDa band was weak (HD-MAR, HT-1) or absent (SUP-T1), indicating translocation-driven expression therein (Figure 2b). N-truncated NTMs in both t(9;14) cells undercut 116 kDa wild-type polypeptide (Figure 2a top), in contrast with t(7;9) SUP-T1 cells, which also translated longer species implying impaired cleavage therein. Correspondingly, ~110 TM/RAM+ forms in t(9;14) cells are taken to represent ICN1. Weak TM/RAM signals in *cis*-HD breakpoint SUP-T1 cells (Figure 2a bottom) also imply impaired GS-cleavage, as Ab8925 epitopes require prior GS exposure. These findings, linking peri-HD breakpoint location to aberrant protein expression, prompted further investigation into the effect of GSi treatments on NOTCH1 signaling and proliferation.

γ-Secretase inhibitor treatment effected dose-dependent reductions of cell growth and viability in HD-MAR and HT-1,

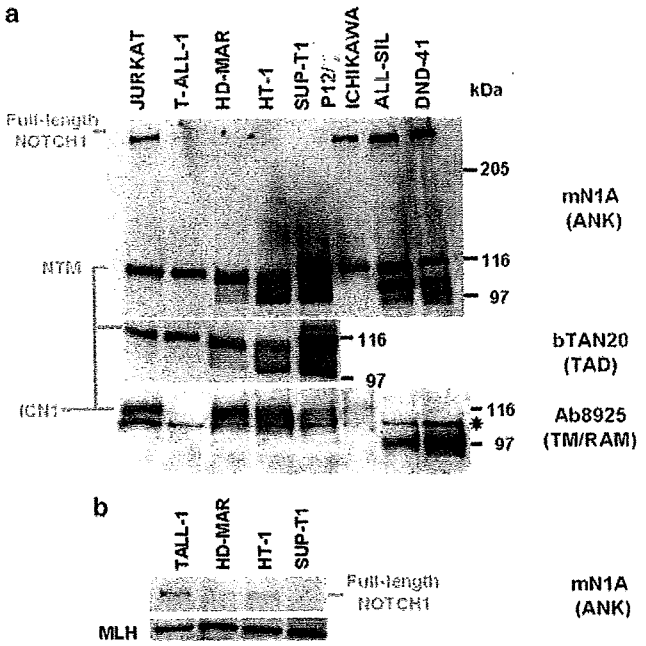

Figure 2 NOTCH1 protein expression in T-cell acute lymphocytic leukemia (T-ALL) cell lines with t(9;14). (**a**) Western analysis of T-ALL cell lines: NOTCH1-ANK domain antibody (Ab) to mN1A (top), bTAN20 Ab to transcriptional activation domains (TADs) (middle) and Ab8925 (activated NOTCH1) to TM/RAM (regulator of amino acid metabolism) (bottom). Ab8925 epitopes include a non-specific band (star) and require prior γ-secretase exposure (manufacturer's data). Note the weak TM/RAM epitopes in SUP-T1 NTM, which are attributable to impaired γ-secretase cleavage. (**b**) Western analysis of full-length NOTCH1 at longer exposure: note the faint (HD-MAR/HT-1) or absent (SUP-T1) full-length NOTCH1 bands, implying translocation-driven expression. Western blots were performed after lysis with 50 μl of RIPA buffer (1 μl aprotinin (1 mg/ml), 5 μl PMSF (20 ng/ml) and 50 μl 2 × SDS). Antibodies used: NOTCH1 (mN1A; BD Biosciences, San Diego, CA, USA, bTAN-20; Hybridoma Bank, Iowa City, IA, USA and Ab8925; Abcam, Cambridge, UK). Loading was checked using Ponceau dye and anti-human-MSH6 Ab (Santa Cruz Biotechnology, Heidelberg, Germany).

while sparing SUP-T1 cells (Figure 3a). The GSi sensitivities of both t(9;14) cell lines significantly exceeded that of T-ALL1, which was described earlier as sensitive.[3] Proliferation arrest in HD-MAR and HT-1 paralleled dose-dependent increases in G0/G1 arrest after GSi treatments, which evinced progressively weaker responses in TALL-1 and SUP-T1 cells (Figure 3b). To investigate these differential GSi sensitivities, downregulation of NOTCH1 transcriptional target genes, HES1 and MYC were respectively, measured in HD-MAR (92, 66%), HT-1 (94, 79%) and SUP-T1 (75, 39%) cells. Differential Gsi sensitivities of NOTCH1 effector gene expression thus paralleled both cell survival and cell cycle progression endpoints (Figures 3c and d), confirming the greater GS-dependence of NOTCH1 signaling in intra-HD breakpoint cells.

Inhibiting cleavage by GS-dependence (GSi) treatment effected the accumulation of four ANK+ species (105–116 kDa) taken as NTM/NTM*I (Figure 3e brackets), and dissipation of ~110 kDa TM/RAM+ (ICN1), that is, a picture consistent with interconversion. This result underlines the dependence of TM/RAM expression on GS activity in t(9;14) cells. A fifth truncated ~100 kDa NTM/NTM*I accumulated in HT-1 cells (arrow). Immunostaining revealed greater accumulation of

perimembraneous NOTCH1 at the expense of intranuclear forms in HD-MAR than in SUP-T1 (Figure 3f). Taken together, GSi treatments revealed increased dependence of intra-HD breakpoint cells on GS activity for NOTCH1 expression, signaling and proliferation. The enhanced TM/RAM epitope exposure of both t(9;14) cell lines (Figure 2a bottom) suggests a protein structural basis underlying the reduced dependence of GS cleavage on prior S2 cleavage owing to their adjacent breakpoints. The correlation of GS sensitivity with intra-HD breakpoint placement is consistent with data from a second t(7;9) cell line CUTLL1 with an intra-HD breakpoint, also sensitive to GSi.[7]

In T-ALL mutations occur in the F-box protein FBXW7 (alias FBW7, hCdc4), which abrogate its binding to NOTCH1, affecting NOTCH1 longevity and GSi responses. However, analysis of HD-MAR, HT-1 and SUP-T1 cells showed normal sequences around Arg465, Arg[479] and Arg[505] hotspots, discounting a major contribution in modulating GSi sensitivity thereby, refocusing the spotlight on GS cleavage.

All the three molecularly karyotyped t(9;14)(q34;q11) cases report TRAD/NOTCH1 involvement (Gesk *et al.*,[8] this report). All the five age-recorded t(9;14) cases were hitherto described in young adults (Table 1), whereas all four t(7;9) cases are pediatric (http://atlasgeneticsoncology.org/), raising the question whether different age groups might be targeted. However, only a few piecemeal cases have been described for either translocation and additional mapped examples are required to delineate breakpoints in both t(9;14) and t(7;9) T-ALL and help determine the clinical relationship of the cytogenetic entities.

Our findings highlight the role of intra-HD NOTCH1 breakpoint locations in promoting ligand-independent transcription and translation of GSi-sensitive polypeptides. Hightened GSi sensitivity bestowed by such intra-HD breakpoints may reflect increased molecular exposure near the HD region facilitating NOTCH1 cleavage. Independence from ligand-mediated cleavage may serve to promote the 'non-oncogene addiction' of intra-HD breakpoint cells on GS cleavage for NOTCH1 signaling.

In summary, we have characterized a new NOTCH1 alteration, t(9;14)(q34;q11), in T-ALL, which is only the second neoplastic NOTCH1 chromosome rearrangement described hitherto. Our data highlight breakpoints in the peri-HD region in determining GS activity and responses to inhibitor. Cell line models for the entity described here provide singular tools for

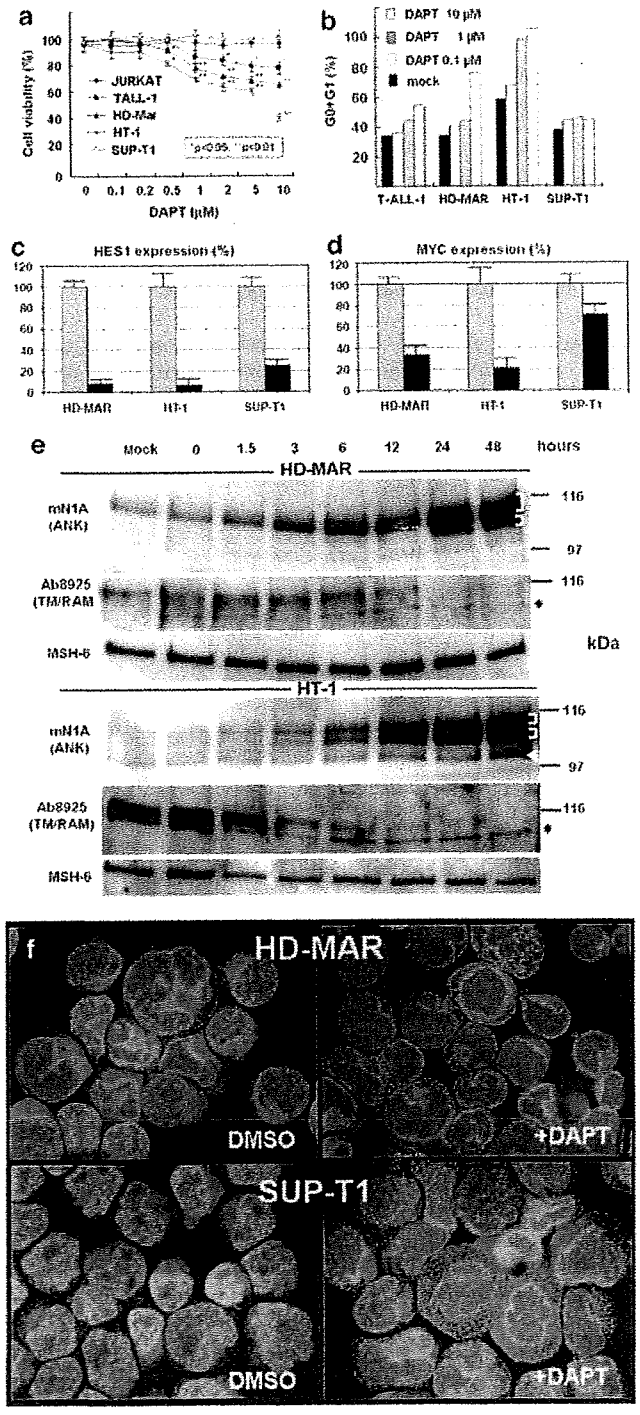

Figure 3 Responses of t(9;14) cells to γ-secretase inhibitors (GSi) treatment .T-ALL cell lines were cultured for 96 h with the indicated concentrations of DAPT or mock-treated with dimethylsulfoxide (DMSO). Cellular proliferation and DNA content were, respectively, measured by 3-(4,5-dimethylthiazol-2-yl)-2,5-diphenyl tetrazolium bromide assay (**a**) and by flow cytometry (**b**) after staining with propidium iodide. Note GSi hypersensitivities of HD-MAR and HT-1 t(9;14) cells at both endpoints. To analyze the effects of GSi on NOTCH1 signaling, t(9;14) and t(7;9) cells were treated for 16 h with 2 μM DAPT and subsequently analyzed by RQ-PCR to measure expression of HES1 (**c**) and MYC (**d**), both shown in black. The DMSO-control was set at 100% (gray). Bars show standard deviations. Again note the greatest HES1/MYC dependence on NOTCH1 signaling in t(9;14) cells. For reverse transcription quantitative (RQ)-PCR, cDNA was synthesized from 5 μg total RNA extracted from 2×10^6 cells with TRIzol (Invitrogen, Karlsruhe, Germany) by random priming in 20 μl using Superscript II (Invitrogen). RQ-PCR used the 7500 Real-Time System (Applied Biosystems, Darmstadt/Germany). Expression of HES1, MYC and the control gene TBP was analyzed using commercial primer sets (Applied Biosystems). To analyse the effects of GSi on NOTCH1 polypeptides, western analysis was performed on HD-MAR and HT-1 cells treated with 2 μM DAPT for the times indicated. (**e**) NOTCH1 polypeptides were immunoprecipitated from whole cell extracts with antibodies recognizing either the intracellular domain of NOTCH1 (mN1A) or the GS-cleaved form of NOTCH1 (ab8925). Brackets show four accumulating ankyrin-positive (ANK+) species (taken as NTM/NTM*I) and concomitant loss of TM/RAM+ (regulator of amino acid metabolism-positive) species (taken as ICN1) following GSi treatment. A fifth truncated ~100 kDa NTM/NTM* accumulated in HT-1 cells (arrow). The starred band is unspecific. (**f**) Effects of GSi on nuclear localization of NOTCH1 polypeptides in HD-MAR and SUP-T1. Cells treated for 24 h with DMSO (left) or 2 μM DAPT (right) were stained with the intracellular domain of NOTCH1 (mN1A) Ab. Reticular staining after GSi treatment reflects the redistribution of NOTCH1 polypeptide to the cell membrane.

Table 1 Summary of t(9;14) cases

Case	Diagnosis	Age (years)	Cell line	Reference
1	T-cell neoplasia[a]	20	HD-MAR	4
2	T-ALL	32	HT-1	5
3	T-ALL	24	—	8
4	T-ALL	23	—	9
5	T-ALL	29	—	9
6	T-CLL	Unknown	—	10

Abbreviations: ALL, acute lymphocytic leukemia; CLL, chronic lymphocytic leukemia; HD, heterodimerization domain.
[a]After Hodgkin's lymphoma.

investigating the leukemic role of NOTCH1, a topic of pressing clinical and scientific interest.

Acknowledgements

We thank H Ben-Bassat and M Abe for HD-MAR and HT-1 cells, respectively, A Ferrando for reading the paper, and the José Carreras Leukemia Research Fund for support.

S Suzuki[1,2], S Nagel[1], B Schneider[1], S Chen[1], M Kaufmann[1], K Uozumi[2], N Arima[2], HG Drexler[1] and RAF MacLeod[1]
[1]*DSMZ, Department of Human and Animal Cell Cultures, Braunschweig, Germany and*
[2]*Center for Chronic Viral Diseases, Kagoshima Univ. Sch. Med. Dent. Sci., Kagoshima, Japan*
E-mail: rml@dsmz.de

References

1 Grabher C, von Boehmer H, Look AT. Notch 1 activation in the molecular pathogenesis of T-cell acute lymphoblastic leukaemia. *Nat Rev Cancer* 2006; **6**: 347–359.
2 Aster JC, Xu L, Karnell FG, Patriub V, Pui JC, Pear WS. Essential roles for ankyrin repeat and transactivation domains in induction of T-cell leukemia by notch1. *Mol Cell Biol* 2000; **20**: 7505–7515.
3 Weng AP, Ferrando AA, Lee W, Morris IV JP, Silverman LB, Sanchez-Irizarry C *et al.* Activating mutations of NOTCH1 in human T cell acute lymphoblastic leukemia. *Science* 2004; **306**: 269–271.
4 Ben-Bassat H, Mitrani-Rosenbaum S, Gamliel H, Naparstek E, Leizerowitz R, Korkesh A *et al.* Establishment in continuous culture of a T-lymphoid cell line (HD-Mar) from a patient with Hodgkin's lymphoma. *Int J Cancer* 1980; **25**: 583–590.
5 Abe M, Tasaki K, Nozawa Y, Tominaga K, Fukuhara S, Ohsato T *et al.* Establishment and characterization of a human T-cell lymphoblastic lymphoma cell line (HT-1) carrying an inversion of chromosome 14. *Cancer* 1992; **69**: 1235–1240.
6 Willis TG, Jadayel DM, Coignet LJ, Abdul-Rauf M, Treleaven JG, Catovsky D *et al.* Rapid molecular cloning of rearrangements of the IGHJ locus using long-distance inverse polymerase chain reaction. *Blood* 1997; **90**: 2456–2464.
7 Palomero T, Barnes KC, Real PJ, Bender JL, Sulis ML, Murty VV *et al.* CUTLL1, a novel human T-cell lymphoma cell line with t(7;9) rearrangement, aberrant NOTCH1 activation and high sensitivity to gamma-secretase inhibitors. *Leukemia* 2006; **20**: 1279–1287.
8 Gesk S, Martin-Subero JI, Harder L, Luhmann B, Schlegelberger B, Calasanz MJ *et al.* Molecular detection of chromosomal breakpoints in T-cell receptor gene loci. *Leukemia* 2003; **17**: 738–745.
9 Clare N, Boldt D, Messerschmidt G, Zeltzer P, Hansen K, Manhoff L. Lymphocyte malignancy and chromosome 14: structural aberrations involving band q11. *Blood* 1986; **67**: 704–709.
10 Zech L, Godal T, Hammarstrom L, Mellstedt H, Smith CI, Totterman T *et al.* Specific chromosome markers involved with chronic T lymphocyte tumors. *Cancer Genet Cytogenet* 1986; **21**: 67–77.

Supplementary Information accompanies the paper on the Leukemia website (http://www.nature.com/leu)

Nuclear entrapment of BCR–ABL by combining imatinib mesylate with leptomycin B does not eliminate CD34$^+$ chronic myeloid leukaemia cells

Leukemia (2009) **23**, 1006–1008; doi:10.1038/leu.2008.367; published online 8 January 2009

Chronic myeloid leukaemia (CML) arises from the formation of the Philadelphia (Ph$^+$) chromosome in haematopoietic stem cells. The translated fusion oncoprotein, BCR–ABL ($p210^{BCR-ABL}$), is a constitutively active tyrosine kinase (TK), which activates multiple proliferative and anti-apoptotic signalling pathways, causing deregulated cell growth.[1] Despite impressive rates of complete cytogenetic response (CCyR) in the majority of patients treated with the targeted TK inhibitor (TKI), imatinib mesylate (IM; Glivec, Novartis, Basle, Switzerland),[2] few patients achieve sustained molecular remission and a significant proportion develops resistance to IM.[3] The presence of pre-existing or acquired BCR–ABL kinase domain mutations, which decrease IM binding,[3] and the innate insensitivity of primitive quiescent CML stem cells to IM[4] are two contributing resistance mechanisms. Consequently, many strategies have been investigated to overcome IM resistance, including the development of second-generation TKIs, nilotinib (Tasigna, Novartis) and dasatinib (Sprycel, Bristol–Myers Squibb, Princeton, NJ, USA), although these remain ineffective against the T315I mutation.

In search of alternative strategies for the elimination of Ph$^+$ cells, Vigneri and Wang [5]showed an intriguing strategy of tricking BCR-ABL$^+$ cells into committing cell death. This mechanism was based on the observation that on treatment with IM, inactive BCR-ABL translocates into the cell nucleus. Entrapment of BCR–ABL there, coupled with re-activation of its TK activity, reversed its role to that of an activator of apoptosis. On the basis of the mounting evidence that BCR–ABL$^+$ stem cells are not eliminated by novel targeted therapies, such as IM and the second-generation TKIs, we investigated whether combination treatment of IM, with the nuclear export inhibitor leptomycin B (LMB Calbiochem), could drive CML CD34$^+$ cells into apoptosis.

Our initial experiments, over a period of 16 days, on the effects of IM, LMB and the combination of these drugs on the Ph$^+$ cell line K562, showed that treatment with either drug alone for the first 72 h was at least cytostatic. However, 5–8 days after drug washout, cells were able to recover, an effect not seen with the drug combination,in which irreversible growth

Bioorganic & Medicinal Chemistry Letters 19 (2009) 3157–3161

Contents lists available at ScienceDirect

Bioorganic & Medicinal Chemistry Letters

journal homepage: www.elsevier.com/locate/bmcl

Discovery of diphenylmethane analogs as anti-bovine diarrhea viral agents

Shinnosuke Hosoda [a,†], Hiroshi Aoyama [a,†], Yukinori Goto [b], Mohammed T. A. Salim [b], Mika Okamoto [b], Mariko Hashimoto [a], Masanori Baba [b,*], Yuichi Hashimoto [a,*]

[a] Institute of Molecular & Cellular Biosciences, The University of Tokyo, 1-1-1 Yayoi, Bunkyo-ku, Tokyo 113-0032, Japan
[b] Division of Antiviral Chemotherapy, Center for Chronic Viral Diseases, Graduate School of Medical and Dental Sciences, Kagoshima University, 8-35-1 Sakuragaoka, Kagoshima 890-8544, Japan

ARTICLE INFO

Article history:
Received 8 April 2009
Revised 28 April 2009
Accepted 29 April 2009
Available online 3 May 2009

Keywords:
Antiviral agents
Bovine viral diarrhea virus
Diphenylmethane

ABSTRACT

Based on antiviral screening of our diphenylmethane derivatives prepared as steroid substitutes, we identified a 1,1-diphenylcyclobutane analog (**9**) and two diethyldiphenylsilane analogs (**12** and **13**) as superior lead compounds with potent anti-bovine viral diarrhea virus (BVDV) activity, having 50% effective concentration (EC_{50}: based on reduction of BVDV replication-induced cell destruction) and 50% cytotoxic concentration (CC_{50}: based on reduction of viable cell number) values of 6.2–8.4 μM and >100 μM, respectively, in Madin–Darby bovine kidney (MDBK) cells infected with BVDV.

HCV infection is thought to be a major cause of human hepatitis globally.[1,2] Currently, the standard treatment for chronic hepatitis C consists of pegylated interferon (IFN)-α in combination with the nucleoside analog ribavirin (1-β-D-ribofuranosyl-1,2,4-triazole-3-carboxamide). However, the virus cannot be eliminated from approximately half of infected patients treated with this combination.[3] Therefore, alternative agents for the treatment and prevention of HCV infection are urgently needed. HCV belongs to the *Flaviviridae* family, as does bovine viral diarrhea virus (BVDV),[1] and because HCV does not replicate efficiently in cell cultures or animals, BVDV is thought to be a good model for human HCV.[4–6]

We have been engaged in structural development studies of anti-BVDV agents based on a γ-carboline skeleton, which was derived from thalidomide.[7,8] These previous studies were inspired by our successful development of α-glucosidase inhibitors derived from thalidomide, because α-glucosidase inhibitors may elicit antiviral activity through inhibition of normal trimming of viral envelope glycoprotein which is necessary for viral maturation/proliferation.[9–11]

On the other hand, we recently reported that some of our α-glucosidase inhibitors derived from thalidomide also act as ligands for liver X receptor (LXR), a member of the nuclear receptor superfamily, whose physiological ligands are oxysterols, including 24(*S*),25-epoxycholesterol (EC) and 22-(*R*)-hydroxycholesterol (HC).[12–15] We also found that several typical synthetic/natural LXR ligands copossess α-glucosidase-inhibitory activity.[13,15] This led us hypothesize a relationship between structures exhibiting α-glucosidase-inhibitory activity and the steroid skeleton; we have also proposed a multi-template hypothesis for molecular design of biologically active compounds.[15,16] The multi-template hypothesis is based on the fact that there exist only a limited number of protein domain folding structures in spite of the existence of a huge number of protein amino acid sequences.[16–18] This hypothesis has led us to design and synthesize various nuclear receptor ligands and steroid-related enzyme inhibitors with a 3,3-diphenylpentane skeleton.[16,19–22] These considerations suggested that 3,3-diphenylpentane and/or related skeleton(s) might be superior multi-templates that can substitute for a steroid skeleton.

In this context, we decided to examine the anti-BVDV activity of our 3,3-diphenylpentane derivatives prepared as nuclear receptor ligands. Anti-BVDV activity of the compounds was evaluated in Madin–Darby bovine kidney (MDBK) cells infected with BVDV (Nose strain), as described previously.[6,23] Here, we report the discovery of anti-BVDV activity of 3,3-diphenylpentane derivatives, as well as structural development studies to increase the activity. The anti-BVDV activity and cytotoxicity of the test compounds are presented as EC_{50} and CC_{50} values, where EC_{50} is the 50% effective concentration based on the reduction of BVDV replication-induced cell destruction, and CC_{50} is the 50% cytotoxic concentration based on the reduction of viable cell number. The selectivity index (SI) is determined as CC_{50}/EC_{50}.

First we screened anti-BVDV activity of our 3,3-diphenylpentane derivatives prepared as nuclear receptor ligands.[19–21] Among these compounds, we found that our potent androgen receptor (AR)/vitamin D receptor (VDR) dual ligand, DPP-0111 (**1**),[20]

* Corresponding authors.
E-mail addresses: m-baba@m2.kufm.kagoshima-u.ac.jp (M. Baba), hashimot@iam.u-tokyo.ac.jp (Y. Hashimoto).
† The first two authors contributed equally.

0960-894X/$ - see front matter © 2009 Elsevier Ltd. All rights reserved.
doi:10.1016/j.bmcl.2009.04.137

possesses moderate but promising anti-BVDV activity with EC_{50}/CC_{50} values of 8.9/82 μM (Fig. 1). Its VDR-selective analog, DPP-1023 (**2**),[20] was also active (EC_{50}/CC_{50} = 25/43 μM), but its anti-BVDV and cytotoxic activities were weaker and stronger than those of **1**, respectively, resulting in a decrease of SI value from 9.21 to 1.72. This result suggests that a hydroxyl group(s) and/or a hydrogen donor(s) on the side chain(s) enhances the cytotoxic activity. Therefore, we prepared the *N*-benzyl analog of **1**, which does not possess a hydrogen donor (**3**: Fig. 1).[24] As expected, the cytotoxic activity of **1** disappeared upon N-benzylation (EC_{50}/CC_{50} = 28/>100 μM), while the anti-BVDV activity of **3** remained (though it was weaker than that of **1**).

To confirm this hydrogen donor effect, several derivatives containing a hydrogen donor(s) (compounds **4–7**) were prepared (Fig. 2), using methods described previously.[19–22,25–28] Briefly, a bisphenol-type core skeleton was prepared by condensation of phenol or *o*-cresol with pentan-3-one or cyclohexanone. Treatment of the obtained bisphenol derivatives with aniline or *o*-toluidine gave core skeletons of **5** and **7**. The phenolic hydroxyl and/or amino group were acylated/alkylated by using usual organic synthetic methods.

All of these compounds (**4–7**) bearing an aryl-XH (X = O or N) group(s) showed moderate (unfavorable) cytotoxic activity with CC_{50} values of 39–50 μM, as expected. Therefore, we chose the bis-pivaloylmethyloxyphenylmethane skeleton for further structural development, and synthesized compounds **8–10** (Fig. 3) using the methods described previously.[19–22,29–31] As expected, compounds **8–10** all showed no apparent cytotoxicity (CC_{50} values of the compounds were all >100 μM) without any decrease of anti-BVDV activity (EC_{50} values of the compounds were 6.3–13.2 μM).

The anti-BVDV activity of compounds **8–10** decreased in the following order: **9** (cyclobutyl) > **8** (dimethyl) ≥ /≈**10** (cyclopentyl). This higher activity of **9** compared with **8** and **10** seems to be attributable to the strained geometry around the quaternary methine carbon atom. Preliminary calculation based on the MMFF 94 force field indicated that the dihedral angle between the two phenyl rings of **9** (106.9°) is smaller than those of compounds **8** and **10** (109–111°) (Fig. 4). Nevertheless, the distance between the two phenyl carbons bound to the methine carbon of **9** (2.61 Å) was calculated to be longer than those of compounds **8** and **10** (2.52–2.55 Å), because of the lengthened C–C bond between the methine carbon and the adjacent phenyl carbon of compound **9**, at least as determined with the MMFF 94 force field calculation method (Fig. 4). Of course, the calculated angles/distances may not be correct, and in fact, other calculation methods, including those based on B3LYP/3-21G, B3LYP/6-31G and MP2/6-31+G*, gave different values individually. However, regardless of the correctness of the calculated values, these considerations led us to design silyl analogs **11–14** (Fig. 5), in which the corresponding dihedral angles and distances were calculated to be 103–104° and 2.98–2.99 Å, respectively, by means of the same MMFF 94 force field-based calculation method (Fig. 4).

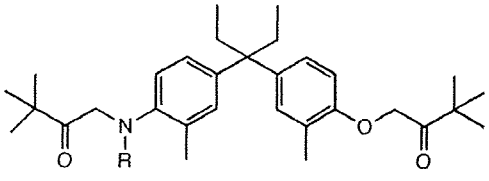

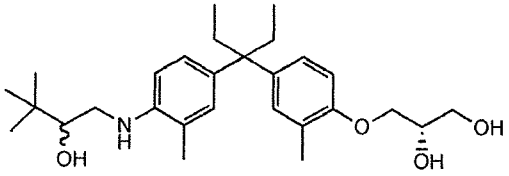

	EC_{50} (μM)	CC_{50} (μM)	SI
1: DPP-0111, R=H	8.9	82	9.21
3: R=Bn	28	>100	-

	EC_{50} (μM)	CC_{50} (μM)	SI
2: DPP-1023	25	43	1.72

Figure 1. Anti-BVDV activity of DPP-0111 (**1**), DPP-1023 (**2**) and *N*-benzyl analog of DPP-0111 (**3**).

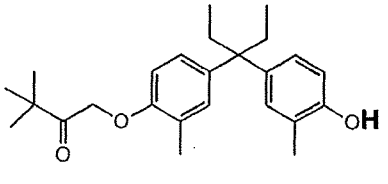

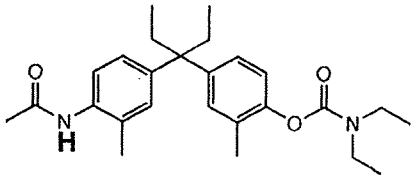

	EC_{50} (μM)	CC_{50} (μM)	SI
4	8.6	45	5.23

	EC_{50} (μM)	CC_{50} (μM)	SI
5	10	50	5.00

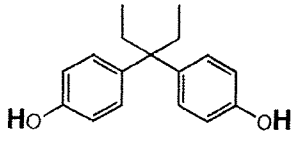

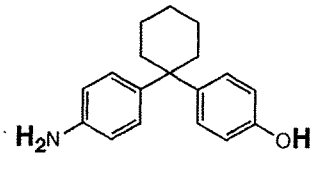

	EC_{50} (μM)	CC_{50} (μM)	SI
6	10	39	3.90

	EC_{50} (μM)	CC_{50} (μM)	SI
7	>42	42	-

Figure 2. Anti-BVDV activity of diphenylpentane derivatives bearing a hydrogen donor group(s).

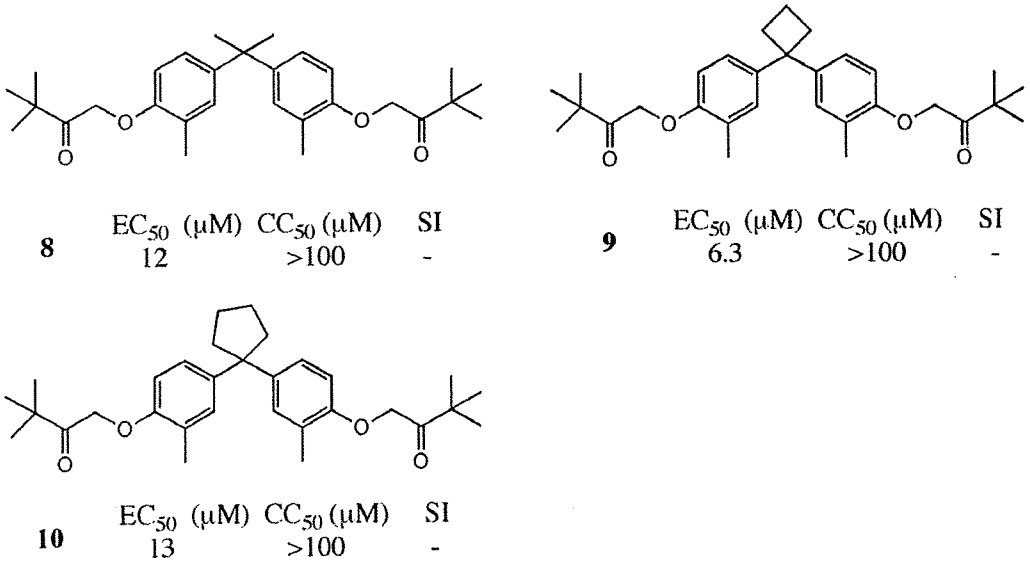

Figure 3. Anti-BVDV activity of bis-pivaloyloxyphenylmethane derivatives.

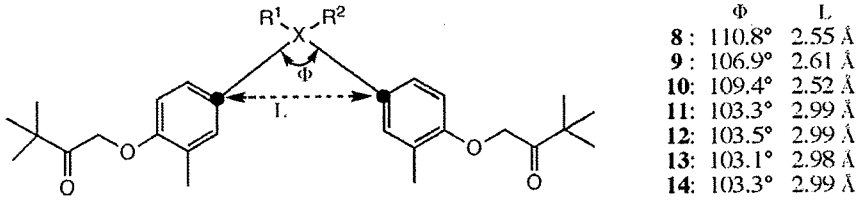

Figure 4. Dihedral angle between the two phenyl rings and distance between the two phenyl carbons bound to the nethine carbon of compounds **8–4** calculated based on MMFF 94 force field.

Compounds **11–14** were synthesized as shown in Scheme 1 by applying the method described by Tagle et al.[32] Briefly, 4-bromo-2-methylphenol (prepared from *o*-cresol by treatment with NBS in CH_3CN) or *p*-bromophenol was reacted with dichlorodiethylsilane or dichlorodimethylsilane in the presence of *n*-BuLi in THF. The resulting bisphenylsilane derivative was further treated with 1-chloropinacolone in the presence of NaH in DMF, giving compounds **11–14**.[33–36] Compound **11** showed similar activity to that

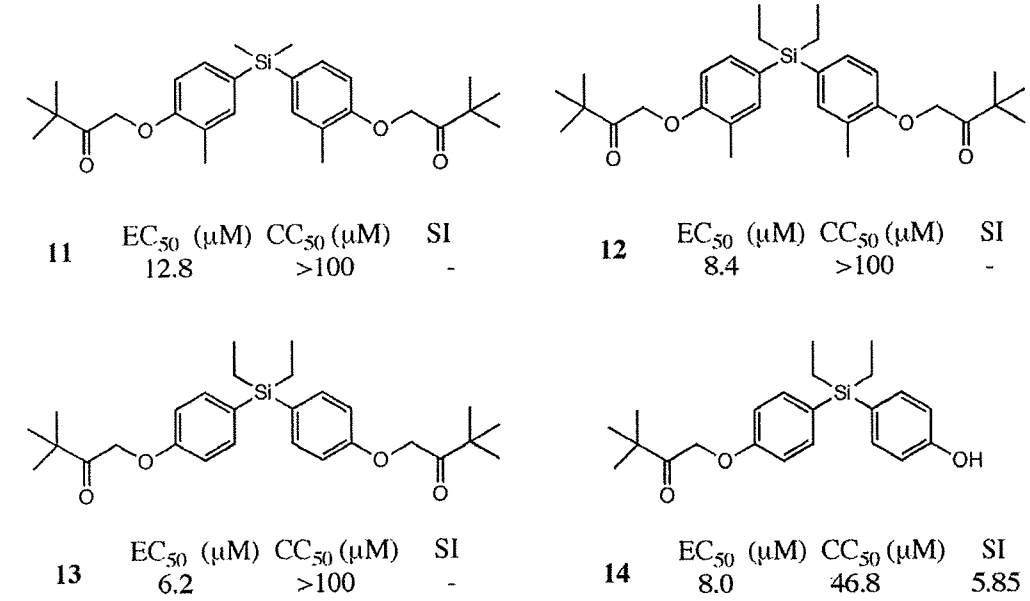

Figure 5. Anti-BVDV activity of bis-pivaloyloxyphenylsilane derivatives.

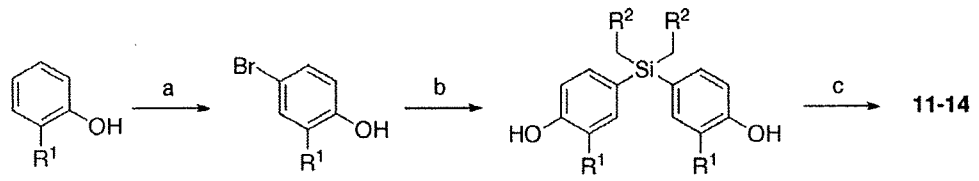

Scheme 1. R^1/R^2 = H or CH_3. Reagents and conditions: (a) NBS, CH_3CN, 75%; (b) *n*-BuLi, $SiEt_2Cl_2$ (or $SiMe_2Cl_2$), THF, 52%; (c) NAH, 1-chloropinacolone, DMF, 19%.

of the corresponding carbon analog **8**, and compounds **12** and **13** showed potent anti-BVDV activity, comparable to that of **9**, with no apparent cytotoxicity, as expected (Fig. 5). In the case of silyl analogs, the existence of a hydroxyl group, that is, compound **14**, resulted in appearance of cytotoxicity, as was the case for the carbon analogs (Fig. 2). The anti-BVDV activity and the cytotoxicity elicited by **14** are similar to those elicited by the corresponding carbon analog **4**. Although we could prepare potent anti-BVDV agents (**12** and **13**) designed based on MMFF 94 force field-based calculation, it was found to be difficult to discuss the observed structure–activity relationships by the use of other calculation methods, including B3LYP/3-21G, B3LYP/6-31G and MP2/6-31+G*. For example, calculation using B3LYP/3-21G gave a quite small differences between the dihedral angles of Ph-C-Ph and Ph-Si-Ph, that is, 110–111° and 109–110°, respectively. The distances between the two phenyl carbons bound to the methine carbon of dimethyl, diethyl, cyclobutyl and cyclopentyl derivatives were calculated to be 2.52–2.54 Å (almost no difference), and those of silyl analogs were calculated to be ca. 3.12 Å by the same B3LYP/3-21G calculation method.

In conclusion, among the compounds presented in this Letter, the cyclobutane analog (**9**) and silyl analogs (**12** and **13**) showed superior activity with EC_{50}/CC_{50} values of 6.3/>100, 8.4/>100 μM and 6.2/>100 μM, respectively. The SI values of these compounds exceeded at least 11.9, suggesting that they represent superior lead compounds for the development of novel antiviral agents. Mechanistic studies, especially identification of the target molecule(s) of compounds **9**, **12** and **13**, are under way.

Acknowledgments

The authors are grateful to Dr. Shinya Usui, Mr. Taniyuki Furuyama and Mr. Kenji Ohgane for helpful discussions and force field calculations. The work described in this Letter was partially supported by the Science and Technology Incubation Program in Advanced Regions, Japan Science and Technology Agency.

References and notes

1. Liang, T. J.; Rehermann, B.; Seeff, L. B.; Hoofnagle, J. H. *Ann. Int. Med.* **2000**, *132*, 296.
2. Hayashi, P. H.; Di Bisceglie, A. M. *Med. Clin. North Am.* **2005**, *89*, 371.
3. McHutchison, J. G.; Gordon, S. C.; Schiff, E. R.; Shiffman, M. L.; Lee, W. M.; Rustgi, V. K.; Goodman, Z. D.; Ling, M. H.; Cort, S.; Albrecht, J. K. *N. Eng. J. Med.* **1998**, 339, 1485.
4. Buckwold, V. E.; Beer, B. E.; Donis, R. O. *Antiviral Res.* **2003**, *60*, 1.
5. Buckwold, V. E.; Wei, J.; Wenzel-Mathers, M.; Russell, J. *Antimicrob. Agents Chemother.* **2003**, *47*, 2293.
6. Yanagida, K.; Baba, C.; Baba, M. *Antiviral Res.* **2004**, *64*, 195.
7. Sako, K.; Aoyama, H.; Sato, S.; Hashimoto, Y.; Baba, M. *Bioorg. Med. Chem.* **2008**, *16*, 3780.
8. Aoyama, H.; Sako, K.; Sato, S.; Nakamura, M.; Miyachi, H.; Baba, M.; Hashimoto, Y. *Heterocycles* **2009**, *77*, 779.
9. Sou, S.; Mayumi, S.; Takahashi, H.; Yamasaki, R.; Ladoya, S.; Sodeoka, M.; Hashimoto, Y. *Bioorg. Med. Chem.* **2000**, *10*, 1081.
10. Takahashi, H.; Sou, S.; Yamasaki, R.; Sodeoka, M.; Hashimoto, Y. *Chem. Pharm. Bull.* **2000**, *48*, 1494.
11. Hashimoto, Y. *Bioorg. Med. Chem.* **2002**, *10*, 461.
12. Noguchi-Yachide, T.; Aoyama, A.; Makishima, M.; Miyachi, H.; Hashimoto, Y. *Bioorg. Med. Chem. Lett.* **2007**, *17*, 3957.
13. Dodo, K.; Aoyama, A.; Noguchi-Yachide, T.; Makishima, M.; Miyachi, H.; Hashimoto, Y. *Bioorg. Med. Chem.* **2008**, *16*, 4272.
14. Noguchi-Yachide, T.; Miyachi, H.; Apyama, A.; Makishima, M.; Aoyama, H.; Hashimoto, Y. *Chem. Pharm. Bull.* **2007**, *55*, 1750.
15. Hashimoto, Y. *Arch. Pharm. Life Sci.* **2008**, *341*, 536.
16. Hosoda, S.; Matsuda, D.; Tomoda, H.; Hashimto, Y. *Mini-Rev. Med. Chem.* **2009**, *9*, 572.
17. Koonin, E. V.; Wolf, Y. I.; Karev, G. P. *Nature* **2002**, *420*, 218.
18. Grishin, N. V. *J. Struct. Biol.* **2001**, *134*, 167.
19. Kainuma, M.; Kasuga, J.; Hosoda, S.; Wakabayasgi, K.; Tanatani, A.; Nagasawa, K.; Miyachi, H.; Makishima, M.; Hashimoto, Y. *Bioorg. Med. Chem.* **2006**, *16*, 3213.
20. Hosoda, S.; Tanatani, A.; Wakabayashi, K.; Makishima, M.; Imai, K.; Miyachi, H.; Nagasawa, K.; Hashimoto, Y. *Bioorg. Med. Chem.* **2006**, *14*, 5489.
21. Hosoda, S.; Hashimoto, Y. *Pure Appl. Chem.* **2007**, *79*, 615.
22. Hosoda, S.; Hashimoto, Y. *Bioorg. Med. Chem. Lett.* **2007**, *17*, 4895.
23. Baba, C.; Yanagida, K.; Kanzaki, T.; Baba, M. *Antiviral Chem. Chemother.* **2005**, *16*, 33.
24. *1-(N-Benzyl-N-(4-(3-(4-(3,3-dimethyl-2-oxobutylhydroxy)-3-methylphenyl)pentan-3-yl)-2-methylphenyl)amino)-3,3-dimethylbutan-2-one* (**3**): Pale yellow amorphous. ^{1}H NMR (500 MHz, $CDCl_3/\delta$): 7.30–7.20 (m, 5H), 7.00 (d, J = 8.6 Hz, 1H), 6.91–6.87 (m, 4H), 6.49 (d, J = 9.4 Hz, 1H), 4.83 (s, 2H), 4.30 (s, 2H), 3.88 (s, 2H), 2.31 (s, 3H), 2.23 (s, 3H), 2.00 (q, J = 7.3 Hz, 4H), 1.25 (s, 9H), 0.99 (s, 9H), 0.57 (t, J = 7.3 Hz, 6H). HRMS (FAB, *m/z*, $[M+H]^+$) calcd for $C_{38}H_{52}NO_3$, 570.3947; found 570.3939.
25. *1-(4-(3-(4-Hydroxy-3-methylphenyl)pentan-3-yl)-2-methylphenoxy)-3,3-dimethylbutan-2-one* (**4**): White crystals. Mp 95–97 °C. ^{1}H NMR (500 MHz, $CDCl_3/\delta$): 691–685 (m, 4H), 6.65 (d, J = 8.1 Hz, 1H), 6.49 (d, J = 8.1 Hz, 1H), 4.83 (s, 2H), 4.50 (s, 1H), 2.23 (s, 3H), 2.19 (s, 3H), 2.00 (q, J = 7.3 Hz, 4H), 1.25 (s, 9H), 0.59 (t, J = 7.3 Hz, 6H). HRMS (FAB, *m/z*, $[M+H]^+$) calcd for $C_{25}H_{34}O_3$, 382.2508; found 382.2508.
26. *4-(3-(4-Acetamido-3-methylphenyl)pentan-3-yl)-2-methylphenyl diethylcarbamate* (**5**): White foam. Mp 58–62 °C. ^{1}H NMR (500 MHz, $CDCl_3/\delta$) 7.66 (d, J = 9.0 Hz, 1H), 7.05 (d, J = 9.0 Hz, 1H), 6.98–6.93 (m, 4H), 6.86 (s, 1H), 3.45 (q, J = 6.8 Hz, 2H), 3.38 (q, J = 6.8 Hz, 2H), 2.19 (s, 3H), 2.19 (s, 3H), 2.15 (s, 3H), 2.04 (q, J = 7.3 Hz, 4H), 1.26 (t, J = 6.8 Hz, 3H), 1.19 (t, J = 6.8 Hz, 3H), 0.59 (t, J = 7.3 Hz, 6H). HRMS (FAB, *m/z*, $[M+H]^+$) calcd for $C_{26}H_{37}N_2O_3$, 425.2804; found 425.2787.
27. *3,3-Bis(4-hydroxyphenyl)pentane* (**6**): White crystals. Mp 201–203 °C. ^{1}H NMR (500 MHz, $CDCl_3/\delta$): 7.02 (d, J = 8.6 Hz, 4H), 6.71 (d, J = 8.6 Hz, 4H), 4.63 (s, 1H), 2.02 (q, J = 7.3 Hz, 4H), 0.60 (t, J = 7.3 Hz, 6H). HRMS (FAB, *m/z*, $[M+H]^+$) calcd for $C_{17}H_{20}O_2$, 256.1463; found 256.1467.
28. *4-(1-(4-Aminophenyl)cyclohexyl)phenol* (**7**): White crystals. Mp 142–143 °C. ^{1}H NMR (500 MHz, $CDCl_3/\delta$): 7.10 (d, J = 8.6 Hz, 2H), 7.04 (d, J = 8.6 Hz, 2H), 6.70 (d, J = 8.6 Hz, 2H), 6.61 (d, J = 8.6 Hz, 2H), 4.77 (br s, 1H), 3.55 (br s, 2H), 2.18–2.05 (m, 4H), 1.53–1.47 (m, 6H). HRMS (FAB, *m/z*, $[M+H]^+$) calcd for $C_{18}H_{21}NO_3$, 267.1623; found 267.1630.
29. *2,2-Bis[4-(3,3-dimethyl-2-oxobutoxy)-3-methylphenyl]propane* (**8**): White crystals. Mp 119–121 °C. ^{1}H NMR (500 MHz, $CDCl_3/\delta$): 6.99 (s, 2H), 6.93 (dd, J = 8.6, 2.6 Hz, 2H), 6.49 (d, J = 8.6 Hz, 2H), 4.84 (s, 4H), 2.25 (s, 6H), 1.59 (s, 6H), 1.25 (s, 18H). ^{13}C NMR (125 MHz, $CDCl_3/\delta$): 210.0, 154.1, 143.5, 129.6, 126.4, 124.7, 110.4, 69.5, 43.2, 41.5, 31.0, 26.3, 16.6. HRMS (FAB, $[M+H^+]$) calcd for $C_{29}H_{41}O_4$, 453.3005, found 453.3011.
30. *1,1-Bis[4-(3,3-dimethyl-2-oxobutoxy)-3-methylphenyl]cyclobutane* (**9**): White solid. Mp 73–75 °C. ^{1}H NMR (500 MHz, $CDCl_3/\delta$): 7.05 (s, 2H), 7.00 (dd, J = 8.6, 2.7 Hz, 2H), 6.52 (d, J = 8.6 Hz, 2H), 4.81 (s, 4H), 2.64 (t, J = 7.7 Hz, 4H), 2.26 (s, 6H), 1.91 (quint, J = 7.7 Hz, 2H), 1.25 (s, 18H). ^{13}C NMR (125 MHz, $CDCl_3/\delta$): 210.0, 154.1, 142.8, 128.9, 126.8, 124.1, 110.8, 69.6, 49.9, 43.2, 35.1, 26.3, 16.6, 16.5. HRMS (FAB, $[M^+]$) calcd for $C_{30}H_{40}O_4$, 464.2927, found 464.2931.
31. *1,1-Bis[4-(3,3-dimethyl-2-oxobutoxy)-3-methylphenyl]cyclopentane* (**10**): White crystals. Mp 68–70 °C. ^{1}H NMR (500 MHz, $CDCl_3/\delta$): 7.01 (s, 2H), 6.98 (dd, J = 8.6, 2.6 Hz, 2H), 6.48 (d, J = 8.6 Hz, 2H), 4.81 (s, 4H), 2.24 (s, 6H), 2.22–2.18 (m, 4H), 1.67–1.65 (m, 4H), 1.24 (s, 18H). ^{13}C NMR (125 MHz, $CDCl_3/\delta$): 210.0, 154.1, 141.8, 129.8, 126.4, 124.8, 110.5, 69.6, 54.3, 43.2, 38.8, 26.4, 23.0, 16.6. HRMS (FAB, $[M^+]$) calcd for $C_{31}H_{42}O_4$, 478.3083, found 478.3104.
32. Tagle, L. H.; Terraza, C. A.; Alvarez, P. *Phosphorus Sulfur Silicon* **2006**, *181*, 239.
33. *Bis(3-methyl-4-(3,3-dimethyl-2-oxobutoxy)phenyl)dimethylsilane* (**11**): White crystals. Mp 120–122 °C. ^{1}H NMR (500 MHz, $CDCl_3/\delta$): 7.27 (s, 2H), 7.23 (d, J = 7.9 Hz, 2H), 6.58 (d, J = 7.9 Hz, 2H), 4.87 (s, 4H), 2.28 (s, 6H), 1.25 (s, 18H), 0.46 (s, 6H); HRMS (FAB, *m/z*, $[M]^+$) calcd for $C_{28}H_{40}O_4Si$, 468.2696; found 468.2700.

34. *Bis(3-methyl-4-(3,3-dimethyl-2-oxobutoxy)phenyl)diethylsilane* (**12**): White crystals. Mp 88–91 °C. ^{1}H NMR (500 MHz, $CDCl_3/\delta$): 7.25 (s, 2H), 7.22 (d, J = 8.5 Hz, 2H), 6.59 (d, J = 8.5 Hz, 2H), 4.87 (s, 4H), 2.28 (s, 6H), 1.26 (s, 18H), 0.99–0.97 (m, 10H); HRMS (FAB, m/z, $[M]^+$) calcd for $C_{30}H_{44}O_4Si$, 496.3009; found 496.2995.
35. *Bis(4-(3,3-dimethyl-2-oxobutoxy)phenyl)diethylsilane* (**13**): White crystals. Mp 40–42 °C. ^{1}H NMR (500 MHz, $CDCl_3/\delta$): 7.39 (d, J = 8.5 Hz, 4H), 6.85 (d, J = 8.5 Hz, 4H), 4.87 (s, 4H), 1.25 (s, 18H), 1.01–0.97 (m, 10H); HRMS (FAB, $[M^+]$) calcd for $C_{28}H_{40}O_4Si$, 468.2696, found 468.2700.
36. *(4-(3,3-Dimethyl-2-oxobutoxy)phenyl)(4-hydroxyphenyl)diethylsilane* (**14**): Coloress oil. ^{1}H NMR (500 MHz, $CDCl_3/\delta$): 7.49 (d, J = 8.5 Hz, 2H), 7.36 (d, J = 8.5 Hz, 2H), 6.89 (d, J = 8.5 Hz, 2H), 6.82 (d, J = 8.5 Hz, 2H), 4.89 (s, 2H), 4.79 (s, 1H), 1.26 (s, 9H), 1.02–0.95 (m, 10H); HRMS (FAB, $[M^+]$) calcd for $C_{22}H_{30}O_3Si$, 370.1964, found 370.1967.

Antiviral Chemistry & Chemotherapy 2010 20:193–200 (doi: 10.3851/IMP1528)

Original article

Anti-bovine viral diarrhoea virus activity of novel diphenylmethane derivatives

*Mohammed TA Salim[1], Mika Okamoto[1], Shinnosuke Hosoda[2], Hiroshi Aoyama[2], Yuichi Hashimoto[2] and Masanori Baba[1]**

[1]Division of Antiviral Chemotherapy, Center for Chronic Viral Diseases, Graduate School of Medical and Dental Sciences, Kagoshima University, Kagoshima, Japan
[2]Institute of Molecular and Cellular Biosciences, University of Tokyo, Tokyo, Japan

*Corresponding author: e-mail: m-baba@vanilla.ocn.ne.jp

Background: A number of compounds were examined for their inhibitory effects on bovine viral diarrhoea virus (BVDV), a surrogate model of hepatitis C virus, in cell cultures. Among them, some diphenylmethane derivatives were found to be selective inhibitors of BVDV.
Methods: Determination of compounds for their anti-BVDV activity was based on the inhibition of virus-induced cytopathic effect in Madin–Darby bovine kidney cells and reduction of infectious virus particles in culture supernatants. To gain insight into the mechanism of action, the inhibition of viral entry and RNA synthesis in the host cells was also determined by real-time reverse transcription-PCR.
Results: Among the test compounds, four diphenylmethane derivatives significantly inhibited BVDV replication with a 50% effective concentration ranging between 6.3 and 10.8 μM. They were not cytotoxic at concentrations up to 100 μM. The representative compound, SH-595A, reduced the virus titre of culture supernatants in a dose-dependent manner. In addition, the compound appeared to somewhat affect viral entry to the host cells. Although SH-595A was inhibitory to viral RNA synthesis, the inhibition was achieved only at high concentrations and was not comparable to its antiviral activity.
Conclusions: The novel diphenylmethane derivatives are effective against BVDV replication and might have a unique mechanism of action.

Introduction

Human chronic hepatitis is often caused by persistent infection with hepatitis C virus (HCV). This persistent infection commonly leads to liver fibrosis, cirrhosis and hepatocellular carcinoma [1]. Pegylated interferon-α in combination with the nucleoside analogue ribavirin is currently used for the treatment of HCV infection [2]; however, the treatment outcome is dependent on the genotype of HCV. Indeed, the treatment is not effective in approximately 50% of patients who are infected with genotype 1b. Furthermore, this combination therapy is expensive and is often associated with unacceptable side effects in many patients; therefore, novel therapies aiming at complete and permanent eradication of HCV from the patient are still mandatory.

HCV belongs to the family *Flaviviridae*, which include three genera: hepacivirus, flavivirus and pestivirus. Bovine viral diarrhoea virus (BVDV), a member of the pestivirus genus is a causative agent of mucosal disease in cattle. The virus possesses a positive sense RNA genome of approximately 12.6 kb. All members of *Flaviviridae* share similarities in virion structure, genome organization and replication machinery. Because BVDV shares many important properties with HCV, BVDV provides a surrogate model of HCV [3,4], in particular, for evaluation of antiviral compounds [5]. Both HCV and BVDV utilize an internal ribosomal entry site within the 5′-non-translated region (NTR) for translating the viral polyprotein. Because of some similarities in their non-structural proteins, antiviral agents active against BVDV are likely to inhibit HCV replication.

The subgenomic HCV RNA replicon cell system has been recognized as a useful tool for discovery of novel anti-HCV agents [6,7]. However, this system does not produce infectious progeny; therefore, it cannot be used for the identification and characterization of antiviral agents acting on early and late steps in the viral replication cycle, such as viral attachment, entry, uncoating, maturation or release. In addition, antiviral agents that

Figure 1. Structures of diphenylmethane derivatives

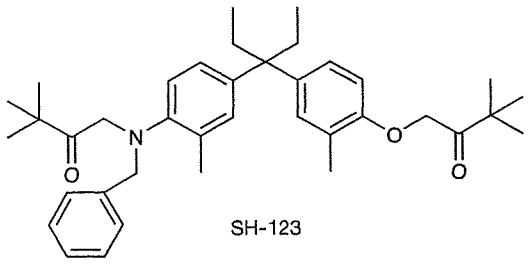

SH-123

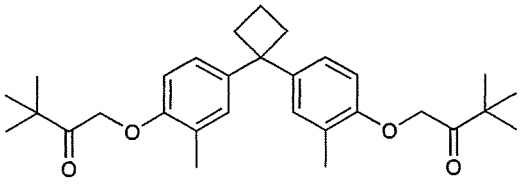

SH-164

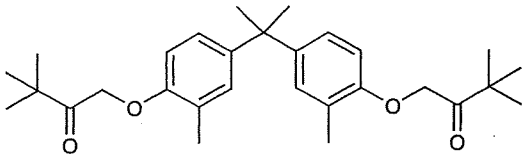

SH-184

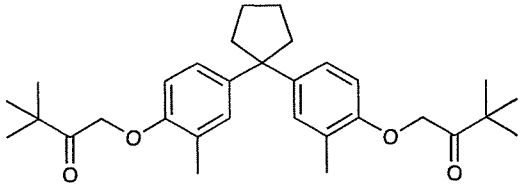

SH-186

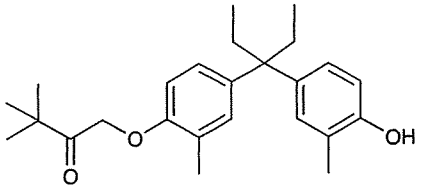

SH-199

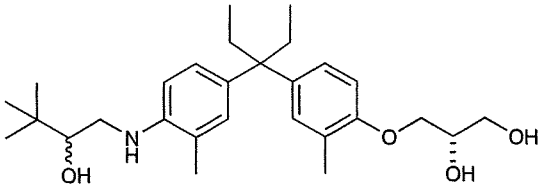

SH-259

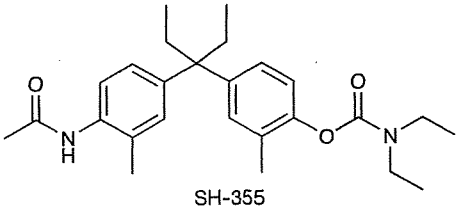

SH-355

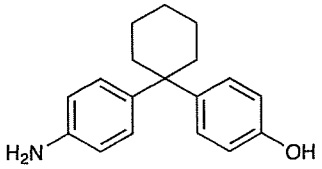

SH-394

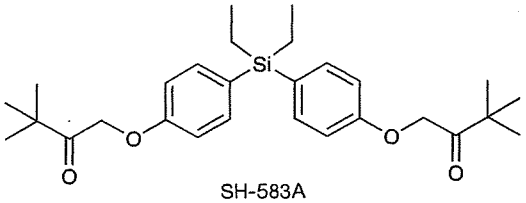

SH-583A

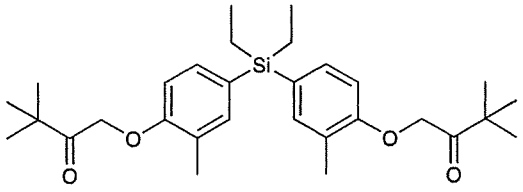

SH-595A

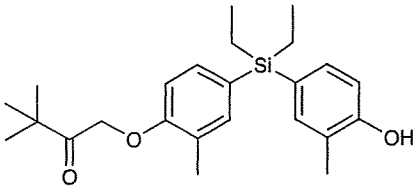

SH-595B

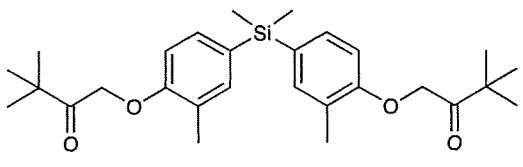

SH-605

reduce the infectivity of progeny cannot be identified in this system [3]. By contrast, a cell culture system of productive HCV infection has recently been established with the replication-competent strain, JFH-1, which makes it possible to identify inhibitors of every step in the viral replication cycle [8–10]. However, this strain was isolated from a patient of fulminant hepatitis C and classified as genotype 2a with several mutations; thus, BVDV is still widely used as a surrogate model for the investigation of anti-HCV agents.

A simple and sensitive colorimetric assay of compounds, which evaluated their anti-BVDV activity, has previously been reported by our group [11]. In this study, we examined novel diphenylmethane derivatives (Figure 1) for their inhibitory effect on BVDV replication and found that some compounds were selective inhibitors of the virus. To gain insight into their mechanism of action, assays for viral entry and RNA inhibition were also conducted.

Methods

Compounds

Twelve diphenylmethane derivatives (Figure 1) and the reference compound, γ-carboline, were selected for antiviral assay. The synthesis of these compounds has been described elsewhere [12,13]. All compounds were dissolved in dimethyl sulfoxide at a concentration of 20 mM and stored at -20°C until use.

Cells and virus

Madin–Darby bovine kidney (MDBK) cells were purchased from Japan Health Sciences Foundation (Health Science Research Resources Bank, Osaka, Japan). The cells were grown and maintained in Dulbecco's modified Eagle's medium with high glucose (4.9 mg/ml; Gibco/BRL, Grand Island, NY, USA). The medium was supplemented with 10% heat-inactivated horse serum (Gibco/BRL), 100 units/ml penicillin G and 100 μg/ml streptomycin. The cells were certified as BVDV-contamination-negative. For antiviral assays, medium supplemented with 3% heat-inactivated horse serum and antibiotics was used. The cytopathic BVDV strain Nose was obtained from Kyoto Biken (Kyoto, Japan). BVDV was harvested from culture supernatants of virus-infected cells after incubation for 3 days. Virus stocks were stored at -80°C until use. The infectivity of the stocks was determined in MDBK cells by an end point serial dilution method and expressed as the 50% tissue culture infectious dose per ml ($TCID_{50}$/ml).

Anti-BVDV assays

Determination of compounds for their anti-BVDV activity was based on the inhibition of virus-induced cytopathic effect (CPE) in MDBK cells, as described previously [11]. Briefly, the cells (1×10^5 cells/ml) were infected with BVDV at a multiplicity of infection (MOI) of 0.01 and 100 μl of the cell suspension was brought into each well in a microtitre plate. The cells were incubated in the presence of various concentrations of test compounds, including the reference compound, γ-carboline, for 3 days at 37°C in a humidified CO_2 incubator. After incubation, culture supernatants were collected to determine their lactate dehydrogenase (LDH) levels by an LDH detection kit (Takara Biochemicals, Otsu, Japan) according the manufacturer's instructions. The cytotoxicity of the compounds was evaluated in parallel with their antiviral activity. The mock-infected MDBK cells (1×10^4 cells/well) were incubated in the presence of various concentrations of test compounds for 3 days. The viability was determined by a dye method using water-soluble tetrazolium Tetracolor One® (Seikagaku Corporation, Tokyo, Japan).

Virus yield reduction assays were conducted for the representative compound, SH-595A, and for γ-carboline. Briefly, MDBK cells (1×10^5 cells/ml) were infected with BVDV at a MOI of 0.01 and 500 μl of the infected cell suspension was brought into each well of a 24-well plate in the presence of various concentrations of SH-595A or γ-carboline. The cells were washed with culture medium at 24 h after virus infection and replaced with fresh culture medium containing appropriate concentrations of the test compounds. The plate was incubated for 2 days at 37°C. The culture supernatant of each well was collected and stored at -80°C until virus titration. The virus titre for each sample was determined and expressed as $TCID_{50}$/ml.

ELISAs

To confirm the anti-BVDV activity of SH-595A, its inhibitory effect on viral antigen production was determined by a BVDV antigen ELISA kit (Bio-X Diagnostics, Jemelle, Belgium). MDBK cells (1×10^4 cells/well) were infected with the virus at a MOI of 0.01 and 100 μl of the cell suspension was brought into each well in a microtitre plate. The cells were incubated in the presence of various concentrations of the compound. After incubation for 3 days at 37°C, the supernatants were collected and their BVDV antigen levels were determined by the ELISA kit according to the manufacturer's instructions.

Real-time reverse transcription-PCR

The anti-BVDV activity of SH-595A and γ-carboline was also determined by the inhibition of viral RNA synthesis in MDBK cells by real-time reverse transcription (RT)-PCR. The cells (2×10^4 cells/well) were infected with the virus at a MOI of 1.0 and cultured in the presence of various concentrations of the test compounds. After incubation for 12 h, the cells

were washed with phosphate-buffered saline (PBS), treated with lysis buffer of TaqMan® Gene Expression Cell-to-CT™ kit (Applied Biosystems, Branchburg, NJ, USA) and subjected to real-time RT-PCR. The BVDV RNA level was determined using the sense primer 5′-TGGTCCGACGCCTTAGTATAAAGG-3′, the antisense primer 5′-GGCTGTATTCGTAAC AGTTGGTTAAA-3′ and the fluorescence probe 5′-ACGAGGGCACGCCCAAAGCA-3′ (Applied Biosystems). The primer pair amplifies the 5′-NTR of BVDV RNA. RT and PCR reagents of the kit were used for real-time RT-PCR according to the manufacturer's instructions. Non-specific inhibition of host cellular messenger RNA (mRNA) synthesis by SH-595A and γ-carboline was determined by amplification of a part of the bovine β-actin mRNA using the sense primer 5′-GCC CTGAGGCTCTCTTCCA-3′, the antisense primer 5′-GCGGATGTCGACGTCACA-3′ and the fluorescence

Figure 2. Inhibitory effect of diphenylmethane derivatives and γ-carboline on BVDV replication in MDBK cells

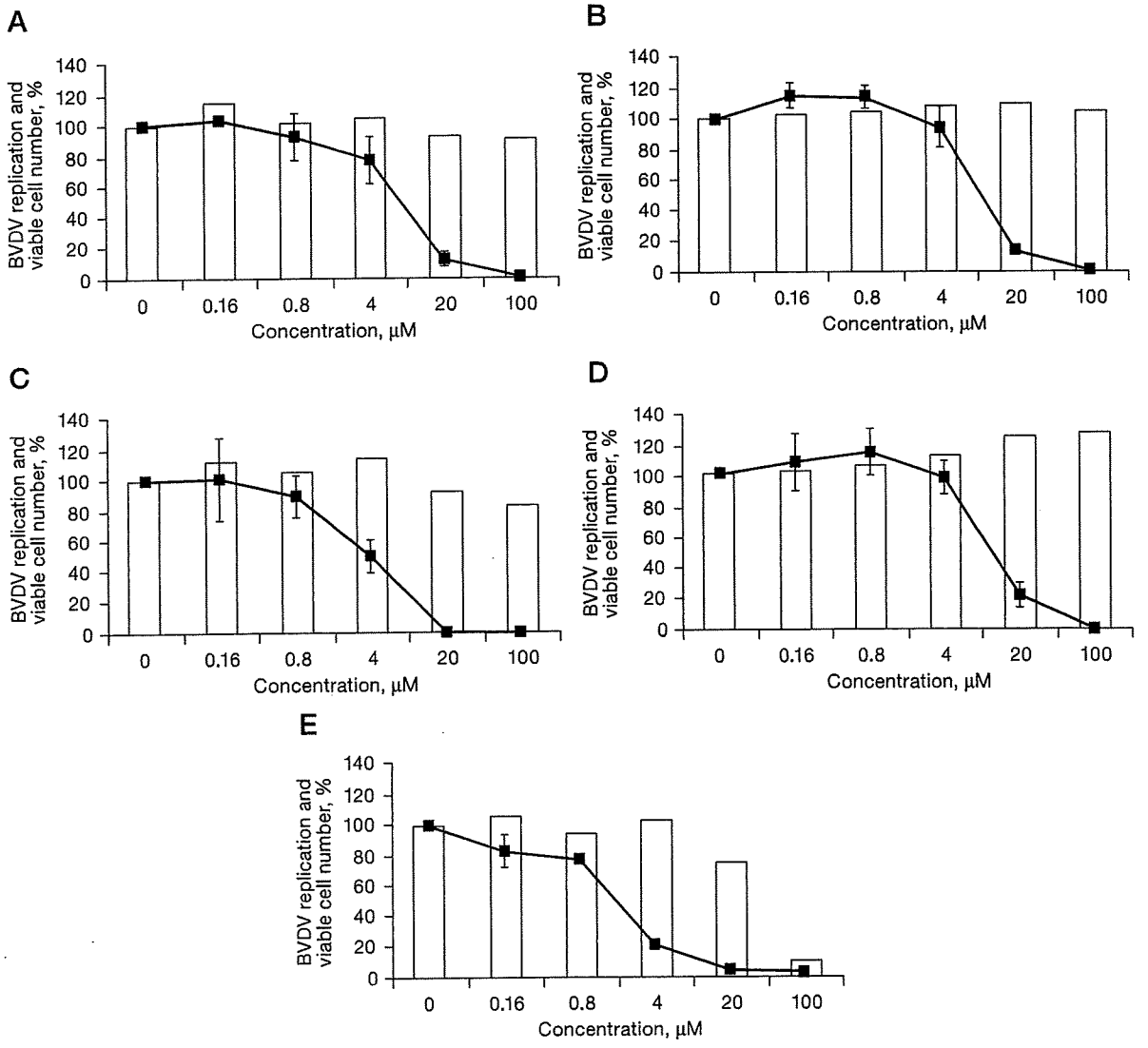

Madin–Darby bovine kidney (MDBK) cells were infected with bovine viral diarrhoea virus (BVDV) at a multiplicity of infection of 0.01 and incubated in the presence of various concentrations of (A) SH-164, (B) SH-184, (C) SH-583A, (D) SH-595A or (E) γ-carboline for 3 days. Lines indicate the virus-induced cytopathic effect in infected cells, as determined by the lactate dehydrogenase method. Columns indicate the viable cell number of mock-infected cells, determined by the tetrazolium dye method. Experiments were repeated at least twice for each compound and representative results are shown.

probe 5′-CATGGAATCCTGCGGCATTCACG-3′ (Applied Biosystems).

Viral entry inhibition assays

MDBK cells (2×10^4 cells/well) were seeded in a microtitre plate and incubated at 37°C for 24 h. The cells were infected with BVDV at a MOI of 2.0. SH-595A (100 μM) and γ-carboline (20 μM) were added at the time of infection and incubated without their removal, added at the time of infection but removed after incubation for 2 h, or added only after incubation for 2 h. The cells were incubated for 12 h after viral infection, washed with PBS and subjected to real-time RT-PCR, as described above.

Results

When 12 diphenylmethane derivatives (Figure 1) were examined for their inhibitory effect on BVDV replication in MDBK cells, 4 compounds displayed dose-dependent inhibition of virus-induced CPE (Figure 2). The 50% effective concentrations (EC_{50}) of SH-164, SH-184, SH-583A and SH-595A were 9.0, 10.8, 6.3 and 10.5 μM, respectively (Table 1). None of the compounds reduced the viability of the mock-infected MDBK cells at a concentration of up to 100 μM. Compounds SH-123, SH-186, SH-199, SH-259, SH-355, SH-394, SH-595B and SH-605 also showed some inhibition of BVDV replication; however, their selectivity indices based on the ratio of 50% cytotoxic concentration (CC_{50}) to EC_{50} were marginal. The EC_{50} and CC_{50} values of the reference compound γ-carboline were 1.9 and 42.6 μM, respectively (Table 1). In the next experiment, SH-595A and γ-carboline were examined for whether they could reduce the amount of infectious virus particles in culture supernatants of the cells. Dose-dependent reduction of the virus titre was observed for both compounds (Figure 3). These results indicate that diphenylmethane derivatives selectively inhibit BVDV replication in cell cultures. The antiviral activity of SH-595A against BVDV was also examined by a sandwich ELISA. It reduced the amount of viral antigen in culture supernatants of the infected cells in a dose-dependent manner (Figure 4). Its EC_{50} was 9.2 μM, which is comparable to the EC_{50} obtained by the CPE inhibition assays (Table 1).

When the inhibitory effect of SH-595A and γ-carboline on BVDV RNA synthesis was examined, SH-595A showed modest inhibition of viral RNA synthesis. Although it achieved approximately 70% inhibition of viral RNA synthesis at a concentration of 100 μM, little inhibition was observed at a concentration of 20 μM (Figure 5A). By contrast, γ-carboline almost completely inhibited viral RNA synthesis at 4 μM without affecting β-actin mRNA synthesis (Figure 5B). Considering the finding that both SH-595A and γ-carboline achieved approximately 80% inhibition of BVDV replication at a concentration of 20 and 4 μM, respectively (Figure 2), the mechanism of BVDV inhibition by SH-595A seems to differ from that by

Table 1. Anti-BVDV activity of diphenylmethane derivatives in MDBK cells

Compound	EC_{50}, μM	CC_{50}, μM	SI
SH-123	21.1 ±7.2	>100	>4.7
SH-164	9.0 ±2.7	>100	>11.1
SH-184	10.8 ±2.0	>100	> 9.3
SH-186	67.1 ±2.6	>100	>1.5
SH-199	7.1 ±3.0	45.1 ±4.0	6.4
SH-259	31.7 ±5.7	43.0 ±6.9	1.4
SH-355	12.5 ±3.5	42.6 ±0.6	3.4
SH-394	16.3 ±7.1	42.0 ±7.5	2.6
SH-583A	6.3 ±1.9	>100	>15.9
SH-595A	10.5 ±2.3	>100	>9.5
SH-595B	9.5 ±2.7	46.8 ±1.1	4.9
SH-605	16.9 ±3.9	>100	>5.9
γ-Carboline	1.9 ±0.4	42.6 ±5.5	22.4

All data represent means ±SD for at least three separate experiments. CC_{50}, 50% cytotoxic concentration based on the reduction of viable cell number; EC_{50}, 50% effective concentration based on the reduction of cell destruction induced by bovine viral diarrhoea virus (BVDV) replication; MDBK, Madin–Darby bovine kidney; SI, selectivity index (a ratio of CC_{50} to EC_{50}).

Figure 3. Inhibitory effect of SH-595A and γ-carboline on viral infectivity in culture supernatants

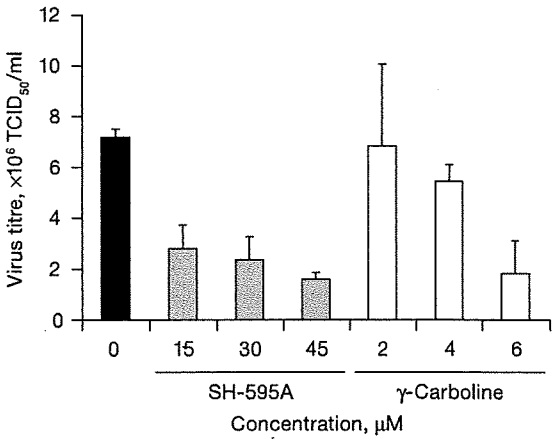

Madin–Darby bovine kidney cells were infected with bovine viral diarrhoea virus at a multiplicity of infection of 0.01 and incubated in the presence of various concentrations of SH-595A or γ-carboline for 24 h. The cells were washed with culture medium and replaced with fresh culture medium containing appropriate concentrations of the test compounds. The plate was further incubated for 2 days. The culture supernatant of each well was collected and, its virus titre was determined and expressed as the 50% tissue culture infectious dose per ml ($TCID_{50}$/ml). All data represent means ±SD for triplicate experiments.

Figure 4. Inhibitory effect of SH-595A on viral antigen production in culture supernatants

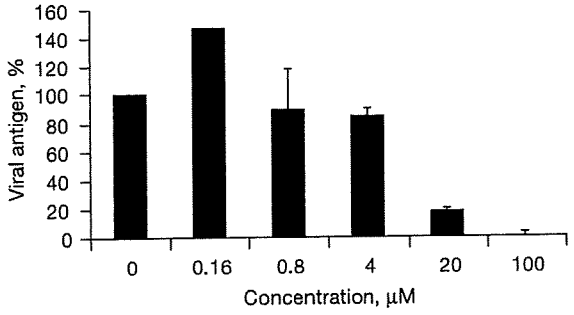

Madin–Darby bovine kidney cells were infected with the bovine viral diarrhoea virus (BVDV) at a multiplicity of infection of 0.01 and incubated in the presence of various concentrations of the compound. After incubation for 3 days, the supernatants were collected and their viral antigen levels were determined by a BVDV antigen ELISA kit (Bio-X Diagnostics, Jemelle, Belgium). All data represent means ±SD for triplicate experiments.

γ-carboline. To gain further insight into the mechanism of BVDV inhibition by SH-595A, the effect of delayed compound addition on the viral RNA synthesis was investigated. The concentrations 100 and 20 μM were used for SH-595A and γ-carboline, respectively. When the compounds were added to the cell cultures simultaneously with the virus and were not removed during the whole culture period (condition 1), 87% and almost complete inhibition of viral RNA synthesis was observed for SH-595A and γ-carboline, respectively (Figure 6). When the compounds existed in the cell cultures during only the first 2 h after virus infection (condition 2), SH-595A and γ-carboline generated 47% and 19% inhibition, respectively. When the compounds were added after the virus adsorption period for 2 h (condition 3), SH-595A and γ-carboline achieved 64% and almost complete inhibition of viral RNA synthesis, respectively. Again, these results indicate that the mechanism of BVDV inhibition by SH-595A seems to differ from that by γ-carboline and that it might interfere with the viral adsorption step to some extent in addition to a step after virus adsorption.

Discussion

BVDV is considered to be a valuable surrogate for identifying and characterizing anti-HCV agents [14]. Our strategy is to discover novel anti-BVDV compounds that can be developed as anti-HCV agents. Recently, we have reported the synthesis of novel diphenylmethane derivatives having anti-BVDV activity in cell cultures [12]. In this study, we attempted to further investigate their antiviral activity and mechanism of action.

Figure 5. Inhibitory effect of SH-595A and γ-carboline on viral RNA synthesis in MDBK cells

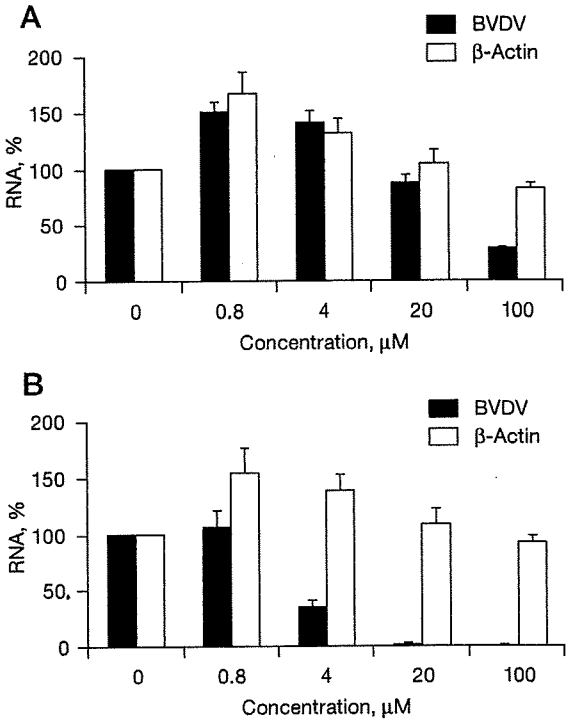

Madin–Darby bovine kidney (MDBK) cells were infected with the bovine viral diarrhoea virus (BVDV) at multiplicity of infection of 1.0 and cultured in the presence of various concentrations of (A) SH-595A or (B) γ-carboline. After incubation for 12 h, the cells were washed with phosphate-buffered saline, treated with lysis buffer and subjected to real-time reverse transcription–PCR (see *Methods*). All data represent mean ±SD for triplicate experiments.

Among the active compounds, SH-595A has been considered as a representative compound and was compared with γ-carboline [13]. SH-595A contains a silicon atom in its chemical structure; therefore, the compound is indeed novel and unique (Figure 1). According to the results obtained by real-time RT-PCR, SH-595A was found to be a modest inhibitor of BVDV RNA synthesis. It only marginally inhibited viral RNA synthesis at a concentration of 20 μM (Figure 5A), at which the compound achieved approximately 80% inhibition of viral replication as determined by the CPE inhibition assay (Figure 2D) and the viral antigen ELISA for culture supernatants (Figure 4). By contrast, γ-carboline was a potent inhibitor of viral RNA synthesis and its inhibitory concentration for viral RNA synthesis corresponded well with that for viral replication (Figures 2E and 5B). It is assumed that γ-carboline exerts its anti-BVDV activity through the inhibition of viral RNA polymerase